~~CONFIDENTIAL~~

NACA RM A57D11

C3

RESEARCH MEMORANDUM

WIND-TUNNEL TESTS OF THE STATIC LONGITUDINAL CHARACTERISTICS AT LOW SPEED OF A SWEPT-WING AIRPLANE WITH BLOWING FLAPS AND LEADING-EDGE SLATS

By Harry A. James and Ralph L. Maki

Ames Aeronautical Laboratory
Moffett Field, Calif.

NATIONAL ADVISORY COMMITTEE FOR AERONAUTICS

WASHINGTON

July 5, 1957

~~CONFIDENTIAL~~

NACA RM A57D11

NATIONAL ADVISORY COMMITTEE FOR AERONAUTICS

RESEARCH MEMORANDUM

WIND-TUNNEL TESTS OF THE STATIC LONGITUDINAL CHARACTERISTICS AT LOW SPEED OF A SWEPT-WING AIRPLANE WITH BLOWING FLAPS AND LEADING-EDGE SLATS

By Harry A. James and Ralph L. Maki

SUMMARY

A wind-tunnel investigation of a high-wing airplane having an aspect ratio 6.75 wing with approximately 36° of sweepback was conducted to determine the lift effectiveness obtainable with trailing-edge blowing flaps in combination with leading-edge slats.

Close to theoretical flap effectiveness was obtained with blowing flaps deflected 45°, 55°, and 65° at low angles of attack. Flap effectiveness and stability were maintained to high angles of attack by control of leading-edge flow separation with slats. Maximum lift was a function of leading-edge configuration, trailing-edge flap deflection angle, and amount of boundary-layer control applied. With a 55° trailing-edge flap, and with a full-span simulated 24° slat, maximum lift coefficient was increased from 2.20 boundary-layer control off to 2.54 with a momentum coefficient of 0.012 and further increased to 2.69 with a momentum coefficient of 0.032.

An evaluation of the results obtained in terms of estimated take-off and landing performance indicated reductions in distance over a 50-foot obstacle amounting to 35 percent on landing and 13 to 18 percent on take-off.

INTRODUCTION

The study at Ames Aeronautical Laboratory of the use of boundary-layer control for increasing lift has included investigations with both area-suction and blowing flaps on a wide range of wing plan forms. It was shown in the tests of reference 1 on an aspect ratio 6.75 wing with approximately 36° of sweepback that flap effectiveness and stability could be maintained to high angles of attack by incorporation of suitable leading-edge devices in combination with highly deflected area-suction flaps. Since questions with regard to the effectiveness of blowing flaps on a swept wing of high aspect ratio remained unanswered, a study was

made to determine the effectiveness of blowing flaps in combination with various leading-edge slats on the same airplane tested in reference 1. Since this airplane incorporates pylon-mounted engine nacelles below and forward of the flapped portion of the wing, a secondary objective was to ascertain the effect of such nacelles on the lift obtained with blowing flaps.

Three-component force and moment data are presented for the airplane equipped with various combinations of leading-edge slats in combination with trailing-edge flaps. Boundary-layer-control flow requirements of the blowing flaps are included for several deflections. All tests were conducted in the 40- by 80-foot wind tunnel of the Ames Aeronautical Laboratory at a Reynolds number of 8.2×10^6 based on the wing mean aerodynamic chord.

An evaluation of some of the results is included in terms of estimated take-off and landing performance for the subject airplane. This evaluation entailed considerations of boundary-layer-control flow requirements, thrust losses, and matching of blowing-flap nozzle size to engine bleed conditions. The methods and assumptions used are outlined in Appendixes A and B.

NOTATION

a	acceleration, ft/sec^2
b	wing span, ft
A_{TP}	cross-sectional area of engine tail-pipe exit, sq ft
c	wing chord, ft
$\bar{c}$	mean aerodynamic chord, $\dfrac{\int_0^{b/2} c^2 dy}{\int_0^{b/2} c\, dy}$, ft
d	perpendicular distance from the plane of the engine thrust axis to the $\bar{c}/4$, ft
F	engine thrust, lb
g	acceleration of gravity, 32.2 ft/sec^2

H	height from ground, ft
K	constant
l	length, ft
M_1	inboard nose glove
M_2	inboard slat
M_3	outboard slat glove
p	static pressure, lb/sq ft
p_t	total pressure, lb/sq ft
$\frac{p_{t_d}}{p_\infty}$	pressure ratio
q	dynamic pressure, lb/sq ft
R	gas constant for air, 1716 sq ft/sec^2 $^\circ$R
s	horizontal distance, ft
S	wing area, sq ft
S_F	wing area subtended by flaps, sq ft
t	time, sec
T	temperature, $^\circ$R
V	velocity, ft/sec
V_{stall}	velocity at $C_{L_{max}}$
V_j	blowing flap jet velocity, $\sqrt{\frac{2\gamma}{\gamma - 1} RT\left[1 - \left(\frac{p_\infty}{p_{t_d}}\right)^{\frac{\gamma-1}{\gamma}}\right]}$, ft/sec
w	specific weight of air, lb/cu ft
W	airplane weight or weight rate of flow, lb or lb/sec
y	spanwise distance measured normal to plane of symmetry, ft

C_D drag coefficient, $\frac{\text{drag}}{q_\infty S}$

C_L lift coefficient, $\frac{\text{lift}}{q_\infty S}$

C_m pitching-moment coefficient referred to axes joining the quarter-chord points of the mean aerodynamic chords of the wing panels, $\frac{\text{pitching moment}}{q_\infty S \bar{c}}$

C_Q flow coefficient, $\frac{W}{wV_\infty S}$

C_μ jet momentum coefficient, $\frac{wV_j}{gq_\infty S}$

C_{P_d} duct pressure coefficient, $\frac{p_{t_d} - p_\infty}{q_\infty}$ for blowing, $\frac{p_\infty - p_{t_d}}{q_\infty}$ for suction

α airplane angle of attack, measured with respect to the fuselage center line, deg

γ ratio of specific heats

δ_f trailing-edge flap deflection angle measured in a plane normal to hinge line, deg

δ_s inboard slat deflection angle measured in a plane normal to hinge line, deg

Δ increment

ϵ engine thrust axis inclination, deg

θ angle of flight path with respect to horizontal, radians

Λ_{HL} angle of sweepback of the flap hinge line, deg

μ rolling or braking coefficient of friction

Subscripts

B engine bleed air

BLC boundary-layer control

d flap duct

[redacted]

E	engine intake air
G	gross
m	flow measuring station
max	maximum
N	net
∞	free stream
TP	tail pipe
TO	take-off
u	uncorrected
v	vertical
1	initial
2	final
2D	two-dimensional
3D	three-dimensional

MODEL AND APPARATUS

Airplane

The test airplane had a high wing of aspect ratio 6.75, 35.92° of sweepback of the quarter-chord line, and an incidence of 4°. Engine nacelles were below and forward of the wing panels at 0.39 semispan. Pertinent geometric details are listed in table I and a sketch of the airplane is presented as figure 1. The angle of attack is referred to the fuselage center line.

Figure 2 is a photograph of the model mounted in the test section. The strut support mounts were attached at the main wheel axles and arrestor-hook pivot point. The bomb-bay doors, nose-wheel door, speed brakes, and the bumper wheel were closed for all tests. The vertical fin was removed at the fold line to provide safe vertical clearance. For the duration of the test, the wing slats were locked in the open position, the horizontal tail was set at an incidence of -4°, and the elevators were locked at 0°. The ailerons were set at 1.5° trim setting (trailing edge up).

[redacted]

Wing leading-edge modifications.- For the portion of the wing inboard of the pylons, a cambered leading-edge glove designated M_1 (more completely described in ref. 1) and a demountable slat designated M_2 as shown in figure 3(a) were made available for these tests. The inboard slat, modification M_2, could be deflected 7.5°, 15°, and 24°. The normal slat for this airplane (outboard of the nacelle pylons) could be modified with a removable glove to simulate a 24° slat deflection, henceforth designated M_3, illustrated in figure 3(a). A photograph of the wing with both slat modifications installed is presented in figure 4.

Trailing-edge flaps.- The single-slotted flaps normally used on this airplane were replaced by the 23-percent-chord plain flaps used in reference 1. However, for this series of tests a blowing boundary-layer control nozzle was incorporated rather than the previously used area-suction screens. A simplified drawing of the nozzle cross section is shown in figure 3(b). The nozzle opening was set at a nominal value of 0.030 inch for these tests.

Engines and ducting.- The J-40 turbojet engines normal for this particular airplane (X model) were replaced by modified J-34 engines as a source of compressed air for the blowing flaps. Air from the last compressor stage of the J-34 turbojet engines was piped to each flap duct via a pipe located just behind the pylons as shown in figure 5. The amount of air delivered to the flaps was controlled by butterfly valves located in this pipe just ahead of the tee connected to the flap ducts.

Engine thrust was determined from static thrust calibrations by means of the wind-tunnel balance system and a single total-pressure probe at the exit of the tail-pipe nozzle of each engine.

TESTS

Range of Variables

The investigation covered a range of angles of attack from -3° to 18° at a constant dynamic pressure of 15 pounds per square foot. This corresponds to a Reynolds number of about 8.2×10^6 based on the mean aerodynamic chord of the wing. The range of flap deflections investigated was from 45° to 65°. The pressure ratio furnished to the nozzles was varied from zero to approximately 2.9. The weight rate of flow was determined from pressure and temperature measurements in the pylon pipes which had been calibrated by means of a standard thin-plate orifice (fig. 5). Total pressure and temperature used for calculation of the jet momentum were measured at the middle and ends of the flap ducts.

Method of Testing

The effects of blowing on the static longitudinal characteristics were determined by pitching the model through the stall with various constant values of momentum coefficient. To ascertain the boundary-layer-control flow requirements, the momentum flow coefficient was varied from zero to a maximum at $\alpha_u = 0^\circ$ for trailing-edge flap deflections of 45°, 55°, and 65°; at $\alpha_u = 8^\circ$ and 10° the boundary-layer-control flow requirements were determined only for a flap deflection of 55°.

CORRECTIONS

Engine Thrust

Since turbojet engines mounted in nacelles were used as a source of high-pressure air for control of the boundary layer over the flaps, it was necessary to correct the measured force and moment data for the effects of engine thrust. The gross thrust based on static-thrust calibration, shown in figure 6, was in good agreement with that computed by the following equation:

$$F_G = KA_{TP}p_{TP}\frac{2\gamma}{\gamma - 1}\left[\left(\frac{p_t}{p}\right)_{TP}^{\frac{\gamma-1}{\gamma}} - 1\right]$$

where K is a calibration constant and was found to be approximately equal to 1.0. With the use of values of total engine air flow, W_E, from unpublished data, the net thrust was defined as

$$F_N = F_G - W_E V_\infty / g$$

The measured coefficients were corrected for the effects of engine thrust by the use of the measured data of figure 6 as follows:

$$C_L = C_{L_u} - \frac{F_N}{q_\infty S}\sin(\alpha + \epsilon)$$

$$C_D = C_{D_u} + \frac{F_N}{q_\infty S}\cos(\alpha + \epsilon)$$

$$C_m = C_{m_u} - \frac{F_N d}{q_\infty S \bar{c}}$$

[redacted]

The force due to turning of the engine inlet air has been omitted since computations indicated that it was negligible.

Tunnel-Wall Corrections

The test airplane was unusually large relative to the tunnel test-section dimensions. The wing-span to tunnel-width ratio was 0.91. Theoretically determined interference effects of the wind-tunnel walls are therefore of doubtful accuracy, but were nevertheless applied to the data. The wall-interference corrections added were as follows:

$$\alpha = \alpha_u + 1.40\ C_{L_u}$$

$$C_D = C_{D_u} + 0.0107\ C_{L_u}{}^2$$

$$C_m = C_{m_u} + 0.039\ C_{L_u}$$

The data have been corrected for stream-angle inclinations. The effects of the tunnel support struts, of removing the vertical fin above the fold line, and of the strut mounting blocks on the main wheel axles are unknown.

RESULTS

The results of force and moment measurements with varying angle of attack for the airplane equipped with various combinations of leading-edge slats and flap deflections are presented in figures 7 through 12. Variations of lift, at constant angle of attack, with momentum, flow, and duct pressure coefficients are shown in figure 13 for constant angles of attack and flap deflection. Data from reference 1 obtained with an area-suction flap are also shown in figures 12, 13(b), and 13(c) for purposes of comparison. Correlations of equivalent two-dimensional momentum coefficient for attached flow with results from reference 2 are shown in figure 14. An evaluation has been made, using the data of figure 15, in terms of estimated performance on take-off and landing and is presented in figures 16 through 19.

DISCUSSION

In general, the effects of changes of leading-edge configuration on the longitudinal characteristics of the airplane with blowing flaps were

[redacted]

found to be similar to those discussed in reference 1 for the airplane equipped with area-suction flaps. The discussion herein, therefore, emphasizes effects peculiar to the blowing-flap installation.

Wind-Tunnel Results

Flap lift.- Incremental lift coefficients due to the flaps were determined from the data of figures 7, 10, and 13(a) at low angles of attack and at C_μ's required for flow attachment on the flaps. These experimentally determined values of lift coefficient are compared in the following table with theoretical values computed by the method presented in reference 3.

δ_f, deg	ΔC_L due to flaps		
	Theory	Measured	
		BLC on	BLC off
45	0.89	0.93	0.60
55	1.11	1.13	.63
65	1.35	1.26	.66

The above correlation with theory indicates that the pylon-mounted engine nacelles probably exerted a negligible effect on the lift effectiveness of the blowing flaps. In the discussion that follows, the maintenance of flap effectiveness to high angles of attack will be shown to be dependent on control of wing leading-edge flow separation. The longitudinal characteristics of the basic configuration (i.e., normal outboard slats extended) with flaps deflected 0° and 55° are presented in figure 7. Close to theoretical flap effectiveness was maintained to an angle of attack of 6° with $C_\mu = 0.012$.[1] At higher angles of attack the losses in lift and marked increases in stability were possibly due to inboard flow separation comparable to that disclosed by tufts during the tests of reference 1. The effect of increasing the momentum from $C_\mu = 0.012$ to 0.032 was to cause a slight increase in lift curve slope and an increase of $C_{L_{max}}$ from 1.78 to 1.94. It was reasoned that further increases of $C_{L_{max}}$ and maintenance of flap effectiveness to angles of attack greater than 6° could be obtained by elimination of inboard flow separation through the use of an inboard slat.

Effects of leading-edge modifications.- The results shown in figure 8 determined for the airplane with an inboard slat indicate that inboard

[1]Examination of static pressure measurements made on the surface of the flaps indicated that $C_\mu = 0.012$ was slightly greater than that required for attached flow on the flaps (see fig. 13(a)).

flow separation was delayed to higher angles of attack with increases of inboard slat deflection angle. A 24° deflection of the inboard slat maintained the flap effectiveness to $\alpha = 10^\circ$ and increased the $C_{L_{max}}$ from 1.78 to 2.32. The adverse variations of stability close to $C_{L_{max}}$ with increases of inboard slat deflection were interpreted as an alleviation of inboard flow separation along with a predominance of outboard (tip) flow separation. The data of reference 4 would indicate that a higher slat deflection than the 17° normally used on this airplane could be expected to provide more effective control of flow separation on the outboard portions of the wing.

The characteristics of the airplane with trailing-edge flaps deflected 55° in combination with a simulated full-span slat deflected 24° are shown in figure 9. A $C_{L_{max}}$ of 2.20 was measured with BLC off which was increased to values of 2.54 at $C_\mu = 0.012$ and to 2.69 with $C_\mu = 0.032$. The flap effectiveness and stability were also maintained up to about 14° angle of attack. No further attempt to find a more effective leading-edge configuration was made since it was indicated in reference 4 that 24° was close to an optimum slat deflection.

The characteristics of the airplane with a simulated 24° slat outboard of the pylons in combination with the normal inboard wing leading edge (no slat) shown in figure 10 are close to those of the basic configuration with normal slat extended. This tends to substantiate the assumption made previously that flow separation occurring inboard of the pylons limited maximum lift.

Effects of flap deflection angle.- The longitudinal characteristics of the airplane are shown in figure 11 at several flap deflections ($C_\mu = 0.012$) with a simulated 24° full-span slat. It can be seen that the lift increases obtained with increases of flap deflection angle up to $\delta_f = 65^\circ$ remained essentially constant throughout most of the lift range. Maximum lift coefficient was increased from 2.43 to 2.54 with increase of flap deflection from 45° to 55°; however, no further increase was obtained with a 65° flap deflection. It may be conjectured that further increases in $C_{L_{max}}$ could be obtained with flap deflections greater than 55° if leading-edge flow separation could have been prevented.

Comparisons with area-suction flaps.- A comparison is made in figure 12 of the characteristics of the airplane equipped with either area suction on the flaps (data from ref. 1) or blowing over the flaps. The leading-edge configurations for this comparison consisted of a simulated 24° slat deflection outboard of the pylons (M_3) and a simulated nose flap (glove modification M_1) inboard of the pylons. The most significant difference is reflected at $C_{L_{max}}$ where a value of 2.16 was obtained with area suction and 2.43 with blowing flaps. In each case, the amount of boundary-layer-control air supplied was slightly in excess of that required for attached flow over the flap at a 55° deflection.

[redacted]

Boundary-layer-control flow requirements.- The variation of lift coefficient with blowing momentum, flow, and duct pressure coefficient is shown in figures 13(a), (b), and (c), respectively. These data were obtained with a simulated 24° full-span slat. Minimum values of momentum coefficient for attached flow based on visual examination of flap surface static-pressure measurements are indicated in figure 13(a). Conversion of these values of C_μ for attached flow to "equivalent" two-dimensional values by the expression

$$C_{\mu_{3D}} = \left(C_{\mu_{2D}}\right)\left(\cos^2\Lambda_{HL}\right)\left(S_F/S\right)$$

based on simple sweep theory gives values in good agreement with those from reference 2 as shown in figure 14.

A comparison of flow requirements and duct pressure coefficients for area-suction and blowing flaps can be made in figures 13(b) and (c). This particular comparison pertains only to the specific blowing nozzle with an 0.030-inch opening used in this test, that is, lower or higher flow coefficients would have been obtained with smaller or larger nozzle openings, respectively. Although the flow coefficients for both types of boundary-layer control were similar for the subject comparison, the much higher pressures associated with the blowing flap shown in figure 13(c) are an indication of higher power requirements for blowing flaps. The same conclusion was reached in reference 2 in a similar comparison.

PERFORMANCE ANALYSIS

An evaluation of the wind-tunnel results in terms of take-off and landing performance is made for the subject airplane equipped with two Pratt and Whitney J-57, 10,000-pound-thrust engines. Data from figure 9 were adjusted for trim by use of tail effectiveness data from reference 1, and are shown in figure 15. Comparisons of the airplane performance, computed from the data of figure 15, are made for boundary-layer control on and off, $\delta_f = 55°$, and with the simulated 24° full-span slat.

The procedure used to estimate bleed flow rates at landing and take-off speeds from various nozzle openings and engine conditions is outlined in Appendix A. The methods and assumptions used for estimating the take-off and landing performance of the airplane are given in Appendix B.

Take-Off Performance

Shown in figure 16 is the variation of take-off distance over a 50-foot obstacle for a wing loading of 90 pounds per square foot. The

speed range, as indicated by the limits of the curves shown in figure 16, corresponds to 1g flight speeds at $\alpha = 2.5^\circ$ to 7°.[2] In the subject performance computations it will be assumed that take-off performed at $\alpha = 2.5^\circ$ is equivalent to "normal" take-off whereas one performed with rotation at take-off up to $\alpha = 7^\circ$ is equivalent to a "short field" take-off. The computed results shown in figure 16 indicate that the blowing flaps could reduce ground roll distance by about 23 percent and could give reductions of 13 to 18 percent on total distance over a 50-foot obstacle.

A summary of take-off performance for a range of wing loadings is shown in figure 17. The results of performance calculations are shown only for 55° flap deflection since calculations for 45° flaps indicated similar performance, whereas those for 65° flaps indicated longer take-off distances than with 55° flaps (boundary-layer control on).

Landing Performance

Shown in figure 18 is the variation of landing distance over a 50-foot obstacle for a wing loading of 64.1 pounds per square foot. The lowest speed shown corresponds to 1g flight at the maximum allowable ground attitude. The results shown in figure 18 indicate a 13-percent reduction in air distance along with a 42-percent reduction of ground roll distance resulting in a net improvement due to blowing flaps of about 35 percent in landing distance over a 50-foot obstacle.

A summary of computed minimum landing distances over a 50-foot obstacle for a range of wing loadings is shown in figure 19. As on take-off, the improvements due to boundary-layer control on were maintained to an almost constant percentage at all the wing loadings shown.

Comparisons With Flight Data

As an indication of the validity of the computation procedures used in the subject performance calculations, a comparison of flight test (ref. 5) and calculated results are shown in figure 20. These calculations involved the use of data from reference 1 for the basic airplane equipped with normal 36° slotted flaps and partial-span slats. The correlation of measured and calculated results is considered to be good since pilot technique, exact flight program, etc., cannot be exactly accounted for in such computations. Landing performance computed by use of an initial sinking velocity of 8.33 feet per second rather than 15.0 feet per second resulted in excellent correlations with the flight data of reference 5.

[2]Normal attitude in ground roll, $\alpha = 2.5^\circ$; maximum safe ground angle, $\alpha = 7^\circ$.

CONCLUSIONS

A low-speed wind-tunnel investigation was conducted on an airplane having an aspect ratio 6.75 wing with 36° of sweepback. It was equipped with trailing-edge blowing flaps and leading-edge slat modifications. Analysis of the data indicates the following conclusions:

1. Close to theoretical flap lift effectiveness was obtained with blowing flaps deflected 45°, 55°, and 65° at low angles of attack.

2. Flap effectiveness and longitudinal stability were maintained to high angles of attack by control of leading-edge flow separation with slats.

3. Maximum lift of the moderately swept high-aspect-ratio wing was a function of leading-edge configuration, trailing-edge flap deflection angle, and amount of boundary-layer-control application. With 55° of trailing-edge flap deflection, and with a full-span simulated 24° slat, maximum lift coefficient was increased from 2.20 with boundary-layer control off to 2.54 with a momentum coefficient of 0.012 and further increased to 2.69 with a momentum coefficient of 0.032.

4. Equivalent two-dimensional values of momentum coefficient for attached flow were in good agreement with values computed by simple sweep theory from results of a previous blowing-flap study.

An evaluation of the results in terms of calculated take-off and landing performance of the subject airplane equipped with a blowing-flap system lead to the following conclusions:

1. Appreciable reductions of both speed and distance required to take-off and land over a 50-foot obstacle should be possible for airplanes with moderately sweptback wings using engine bleed air for blowing flaps.

2. For the subject airplane, calculated reductions in distance over a 50-foot obstacle due to boundary-layer control amounted to 13 to 18 percent on take-off and about 35 percent on landing.

Ames Aeronautical Laboratory
National Advisory Committee for Aeronautics
Moffett Field, Calif., Apr. 11, 1957.

APPENDIX A

DETERMINATION OF ENGINE BLEED RATE AND NOZZLE SIZE

The design of a blowing-flap nozzle involves considerations of allowable flow rates, compressed air source conditions, line losses, etc., to obtain a specified jet momentum coefficient for a range of operational speeds. Like most engineering computations, this will involve compromises in order to obtain a practical design. An example for the subject airplane with a 55° blowing flap using bleed air from J-57 turbojet engines will be used to illustrate a suggested design procedure. The engine thrust and bleed characteristics at standard sea-level conditions from references 6 and 7 will be used in the example computations.

Choice of Design C_μ

A design momentum coefficient close to that required for attached flow should be adequate for preliminary design purposes. This can be estimated by the method of reference 2. When engine bleed air is used, as will be assumed in the subject example, it is desirable to use a minimum amount of bleed so as to minimize thrust losses. This is especially important at take-off. For the subject example, a $C_\mu = 0.011$ was selected for $\delta_f = 55°$ directly from data shown in figure 13(a).

Choice of Design Speeds

Use of the 1.2 V_{stall} criterion for both landing and take-off speeds based on $C_{L_{max}} = 2.42$ from figure 15 for a range of wing loadings of 77 to 102.6 pounds per square foot at take-off and 55 to 77 pounds per square foot at landing indicated a design speed range of 97 to 131 knots. As a compromise the following average speeds were selected for the subject example: landing, 102 knots; and take-off, 120 knots.

Air-Flow Computations

Once values of C_μ and design speeds have been ascertained, use of isentropic relations for air and the fundamental equation

$$C_\mu = \frac{WV_j}{q_\infty S g}$$

can be used to determine the weight rate of flow (see ref. 2).

[redacted]

Choice of Nozzle Size

The flow through the nozzle can be treated as an isentropic process, reference 8, to determine a nozzle size which will supply the required jet momentum for a given set of compressor or source conditions of temperature and pressure. A graph such as is illustrated in figure 21 will be found useful in the selection of a fixed nozzle size as a compromise for a range of speeds and compressor source conditions. The development of such a chart is more completely described in reference 2.

For the subject example, a take-off speed of 120 knots with a pressure ratio of 10 would require a 0.005-inch nozzle to obtain a design C_μ of 0.011. However, use of this nozzle size at landing conditions of 102 knots and pressure ratio of 3.7 would not supply the required jet momentum. As noted in figure 21, a 0.012-inch nozzle is required at the design landing conditions. Conversely, if the larger nozzle (0.012-inch) were used at take-off, a bleed rate of 14.9 pounds per second with an 11-percent thrust loss would result. Engine thrust losses were computed by the method of reference 6. One of the most obvious solutions of this problem is to incorporate a controllable line restriction, such as a two-position valve, along with the larger nozzle size so as to restrict the flow to the flaps to give a design momentum for take-off. For the subject example, the thrust loss was reduced to 5 percent at take-off by assuming that the bleed rate was restricted to 7.0 pounds per second at a pressure ratio of 4.7 with the 0.012-inch nozzle.

In the subject performance calculations, constant bleed rates of 7.0 pounds per second at take-off and 5.4 pounds per second at landing were assumed. This naturally resulted in variations of C_μ and hence C_L at speeds other than 102 knots for landing and 120 knots for take-off. However, even at the highest speeds associated with the highest wing loading (102.6 lb/sq ft) considered herein, the reduction of C_μ from 0.011 to 0.008 resulted in an almost negligible change in C_L as can be seen in figure 13(a).

[redacted]

APPENDIX B

METHODS AND ASSUMPTIONS USED IN PERFORMANCE CALCULATIONS

Take-Off

Ground roll.- The equation used for the computation of ground roll was almost identical to that given in reference 9 with inclusion of $C_{L_G}/C_{L_{TO}}$ in place of L/W and is as follows:

$$s = \frac{13.1(W/S)}{C_{L_G}(D/L - \mu)} \ln\left[\frac{(F/W - \mu)}{(F/W - \mu) - (C_{L_G}/C_{L_{TO}})(D/L - \mu)}\right]$$

The following assumptions have been made:

1. Constant ground-roll attitude, $\alpha = 2.5^\circ$.

2. Airplane rotated at the end of ground roll to any angle between $\alpha = 2.5^\circ$ and 7°.

3. Average thrust through the ground-roll speed range.

4. Effects of engine thrust axis inclination included in lift summation.

5. $\mu = 0.03$.

Air distance.- The method of reference 10 was used to calculate the air distance (transition) to attain an altitude of 50 feet.

$$a_V = g\frac{C_L}{C_{L_{TO}}} \qquad V_V = (F - C_D qS)\frac{V_{TO}}{W}$$

$$\Delta t = \frac{2\Delta V_V}{a_{V_1} + a_{V_2}} \qquad H = \sum\left(\frac{V_{V_1} + V_{V_2}}{2}\right)\Delta t \ldots$$

The following assumptions were made:

1. Flight path restricted to small angle of climb so that $\tan\theta = \sin\theta$ and $\cos\theta = 1$.

[redacted]

2. Constant airspeed.

3. Constant thrust.

4. Flight programmed at one half of the maximum vertical acceleration.

Landing

Ground roll.- The computations for landing ground roll involved the use of the same equation as used for take-off with the addition of the following assumptions:

1. Thrust reduced to idle rpm value at touchdown.

2. Braking coefficient taken from curve shown in figure 22 (see ref. 9).

3. Boundary-layer control was assumed to be shut off during ground roll.

Air distance (flare).- The variable load factor case from reference 11 was used:

$$s = V_1 t_2 \qquad H_1 = -\frac{1}{2} V_{V_1} t_2$$

$$\Delta V_2 = g\left(\frac{F}{W} - \frac{D}{L} - \frac{V_{V_1}}{2V_1}\right)t_2 + \frac{D}{L} V_{V_1}$$

For the flare computations the following assumptions were made:

1. Flight path angle small enough so that $\theta = \sin\theta = V_V/V$ and $\cos\theta = 1$.

2. F/W and D/L assumed to remain constant.

3. Maximum attitude at touchdown restricted to $\alpha = 7^\circ$, maximum safe ground angle.

4. An initial sinking velocity of 15 feet per second was used.

REFERENCES

1. Maki, Ralph L., and James, Harry A.: Wind-Tunnel Tests of the Static Longitudinal Characteristics at Low Speed of a Swept-Wing Airplane With Slotted Flaps, Area-Suction Flaps, and Wing Leading-Edge Devices. NACA RM A57A24, 1957.

2. Kelly, Mark W., and Tolhurst, William H., Jr.: Full-Scale Wind-Tunnel Tests of a 35° Sweptback Wing Airplane With High-Velocity Blowing Over the Trailing-Edge Flaps. NACA RM A55I09, 1955.

3. DeYoung, John: Theoretical Symmetric Span Loading Due to Flap Deflection for Wings of Arbitrary Plan Form at Subsonic Speeds. NACA Rep. 1071, 1952.

4. Kelly, John A., and Hayter, Nora-Lee F.: Lift and Pitching Moment at Low Speeds of the NACA 64A010 Airfoil Section Equipped With Various Combinations of a Leading-Edge Slat, Leading-Edge Flap, Split Flap, and Double-Slotted Flap. NACA TN 3007, 1953.

5. Snawder, Elden J., and Bock, Charles C., Jr.: RB-66B Phase IV Performance Test. AFF TC-TR 56-6, Edwards, Calif., May 1956.

6. Anon.: Model J57-P-1 Engine. Spec. No. A-1632-C, Pratt Whitney Aircraft Co., 25 Aug. 1953.

7. Kelly, Mark W., and Tucker, Jeffrey H.: Wind-Tunnel Tests of Blowing Boundary-Layer Control With Jet Pressure Ratios Up to 9.5 on the Trailing-Edge Flaps of a 35° Sweptback Wing Airplane. NACA RM A56G19, 1956.

8. Staff of the Ames Aeronautical Laboratory: Notes and Tables for Use in the Analysis of Supersonic Flow. NACA Rep. 1135, 1953. (Supersedes NACA TN 1428)

9. Perkins, Courtland D., and Dommasch, Daniel O., eds.: Flight Testing. Vol. I - Performance. AGARD, 1955.

10. Kiehle, M. H., and Vantine, A.: A Consideration of Calculated Versus Flight Test Take-Off Performance. Jour. Aero. Sci., vol. 12, no. 3, pp. 263-272.

11. Fusfeld, Robert D.: A Method of Calculating the Landing Flare Path of an Airplane. Aero. Eng. Review, vol. 10, Feb. 1951, pp. 25-30.

[redacted]

TABLE I.- GEOMETRIC DATA OF UNMODIFIED TEST AIRPLANE

Wing	
Area, sq ft	780
Span, ft	72.5
Aspect ratio	6.75
Taper ratio	0.335
Mean aerodynamic chord, ft	11.68
Sweepback of the quarter-chord line, deg	35.92
Incidence, deg	4.0
Dihedral, deg	0
Twist, deg	0
Airfoil section at root (streamwise)	NACA 63-009.95(mod)
Airfoil section at tip (streamwise)	NACA 63-008.25(mod)
Flap	
Span of one flap, ft	16.84
Inboard end of flap from center line of fuselage, ft	4.00
Flap chord, percent chord (slotted flap)	25
Flap chord, percent chord (plain flap)	23
Slat	
Span of one slat, ft	21.42
Inboard end of slat, feet from fuselage center line	14.14
Slat chord at inboard end, percent chord	16.9
Slat chord at wing tip, percent chord	24.3
Slat deflection, deg	17.0
Horizontal tail	
Area, sq ft	166.6
Span, ft	25.83
Aspect ratio	4.0
Taper ratio	0.50
Mean aerodynamic chord, ft	6.75
Sweepback of the quarter-chord line, deg	33.88
Volume, tail length/$\bar{c}$ × tail area/S	0.531
Dihedral, deg	10.0
Height of tail above wing plane, ft	6.68
Fuselage	
Length, ft	71.19
Frontal area (excluding canopy), sq ft	50.4
Maximum width, ft	7.17
Engine nacelles (J-40)	
Perpendicular distance from engine thrust axes to axis joining the $\bar{c}/4$ points of the wing panels (d), ft	4.44
Engine thrust axis inclination (ϵ), deg	2.50

[redacted]

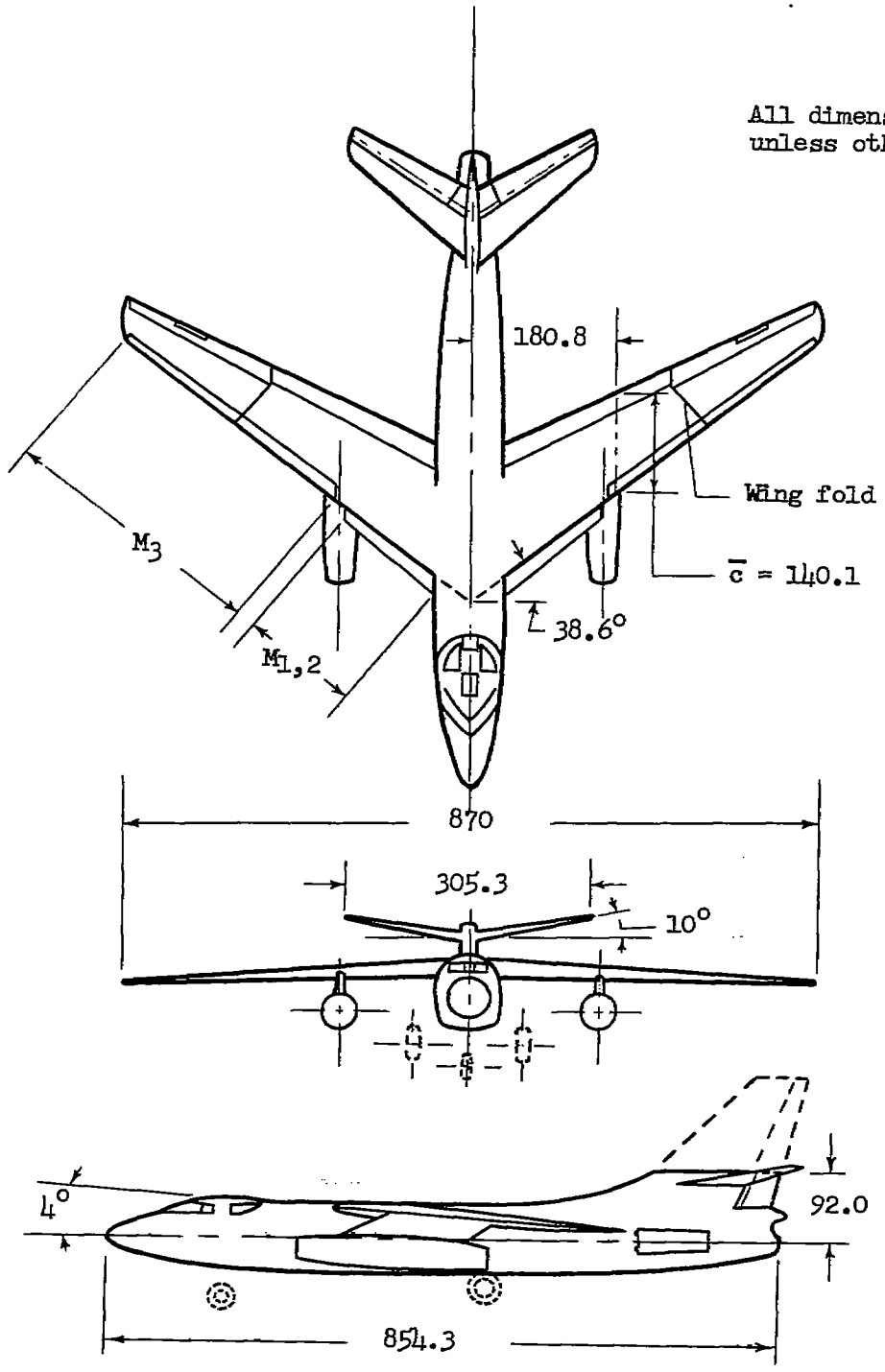

Figure 1.- Three-view sketch of the test airplane.

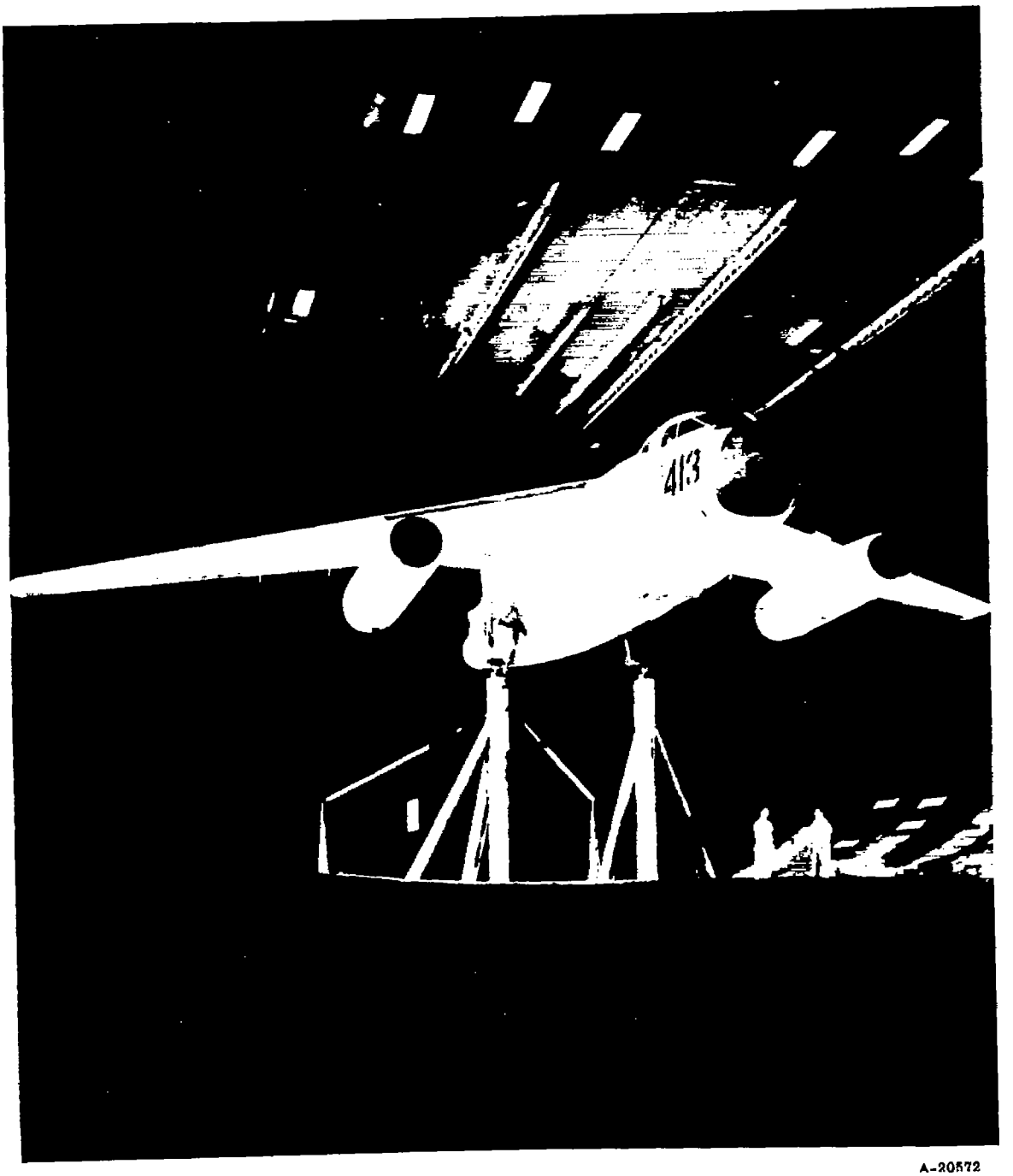

Figure 2.- View of the airplane mounted on the wind-tunnel struts; front view, flaps undeflected.

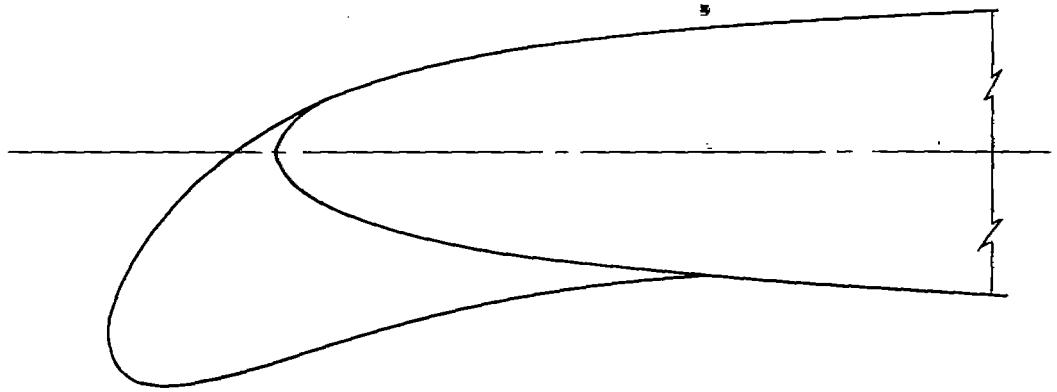

Inboard nose glove, M_1

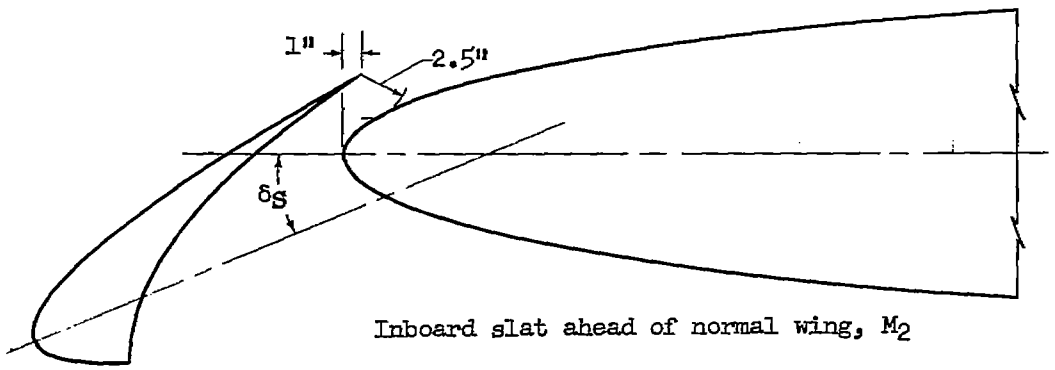

Inboard slat ahead of normal wing, M_2

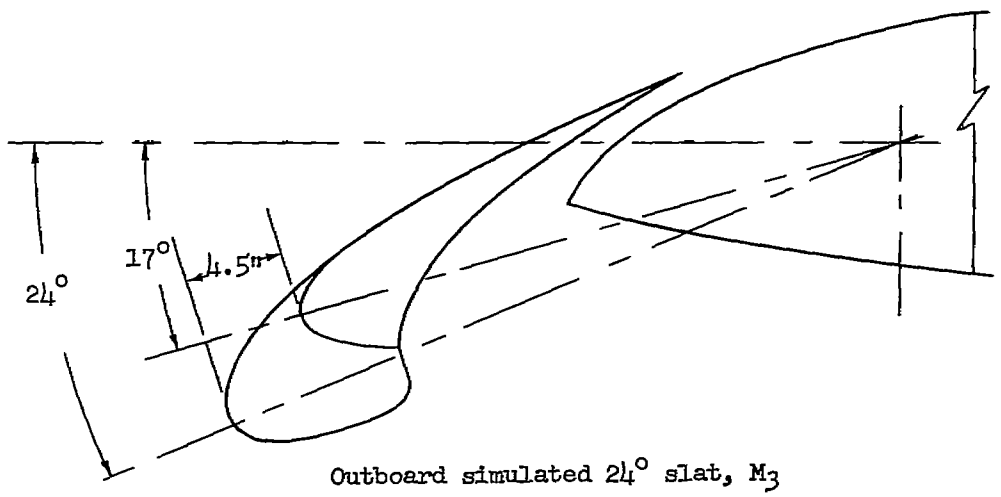

Outboard simulated 24° slat, M_3

(a) Leading-edge modifications.

Figure 3.- Cross-section sketches of the leading-edge slat modifications and blowing flap.

[redacted]

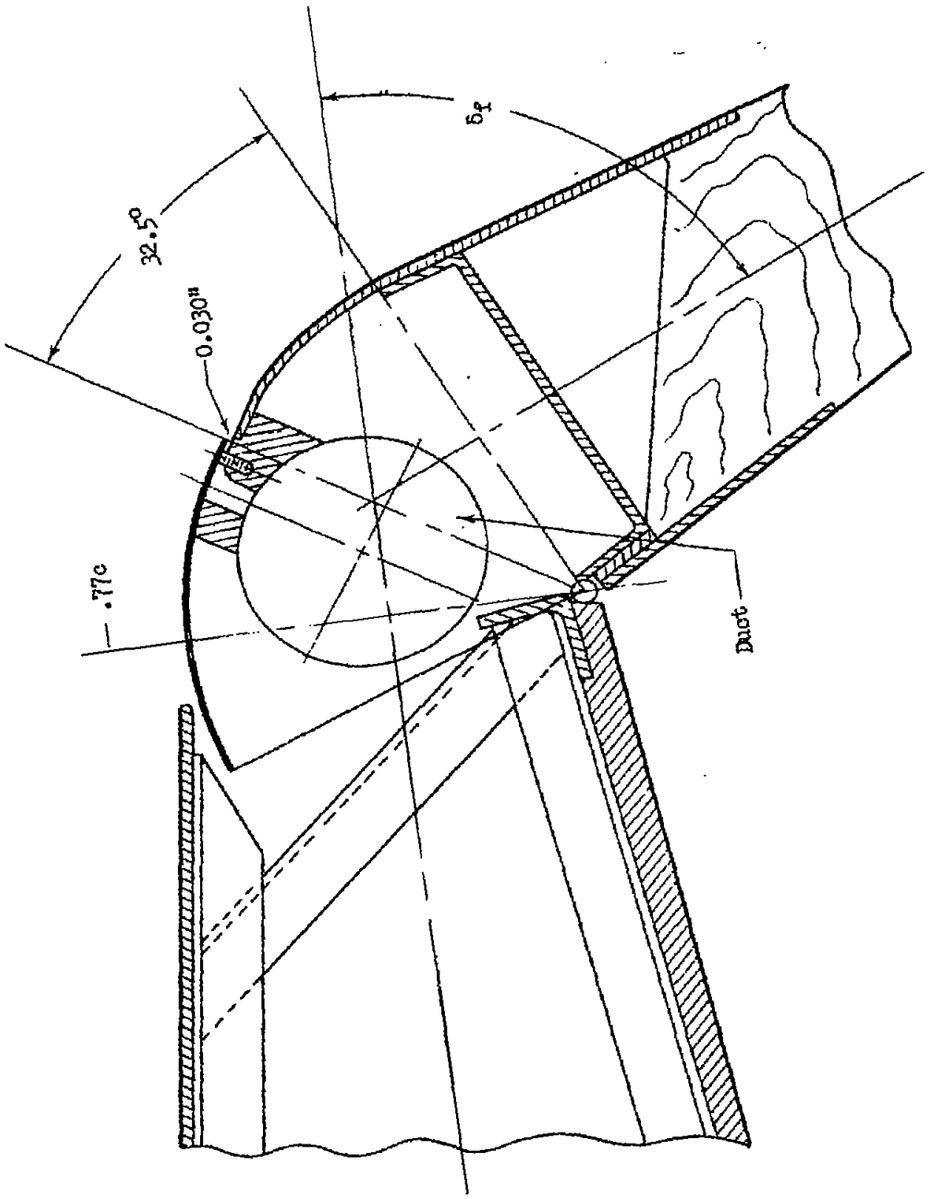

(b) Blowing flap.

Figure 3.- Concluded.

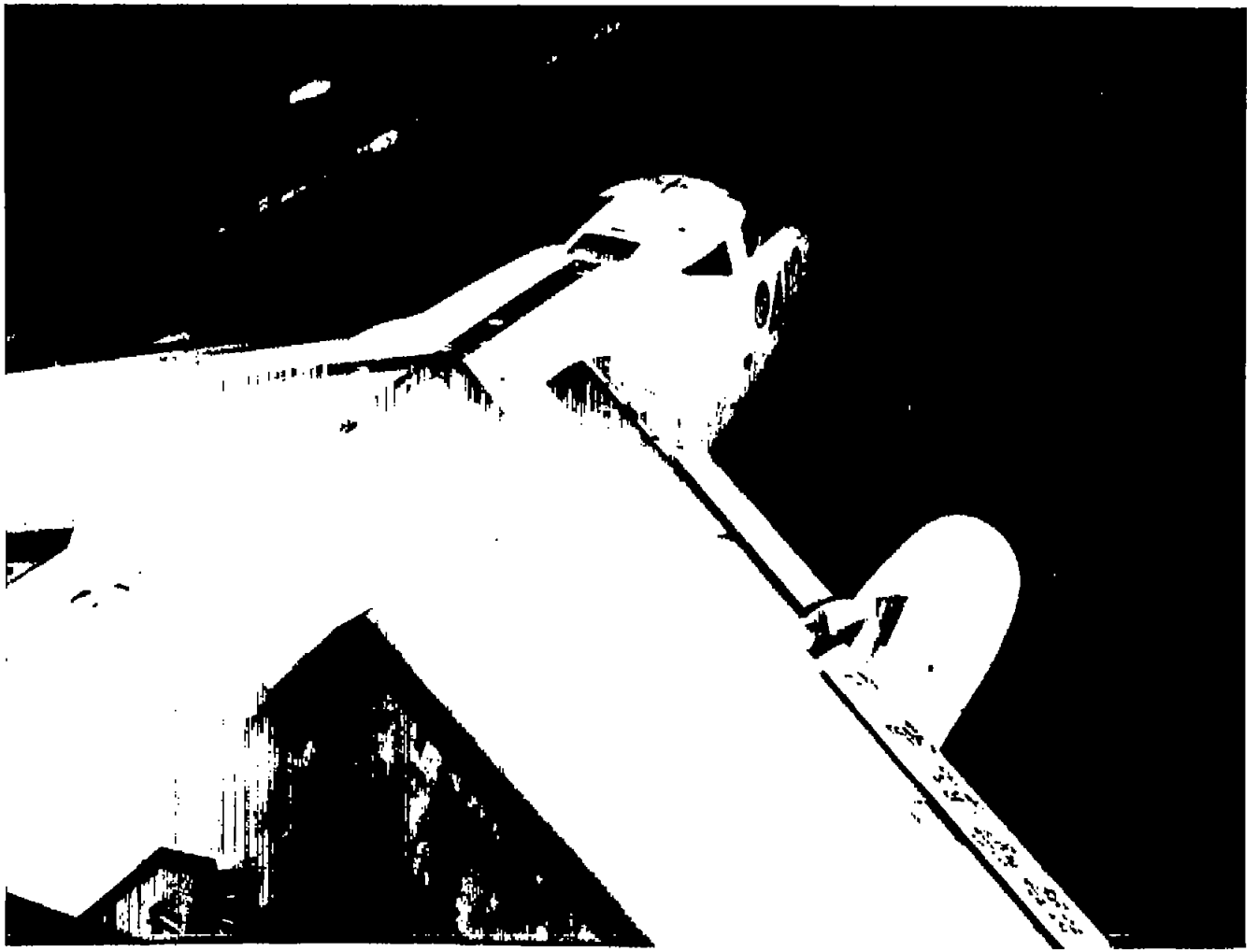

A-21511

Figure 4.- View from above and behind the right wing showing the test airplane with slat modifications installed over the entire exposed wing leading edges.

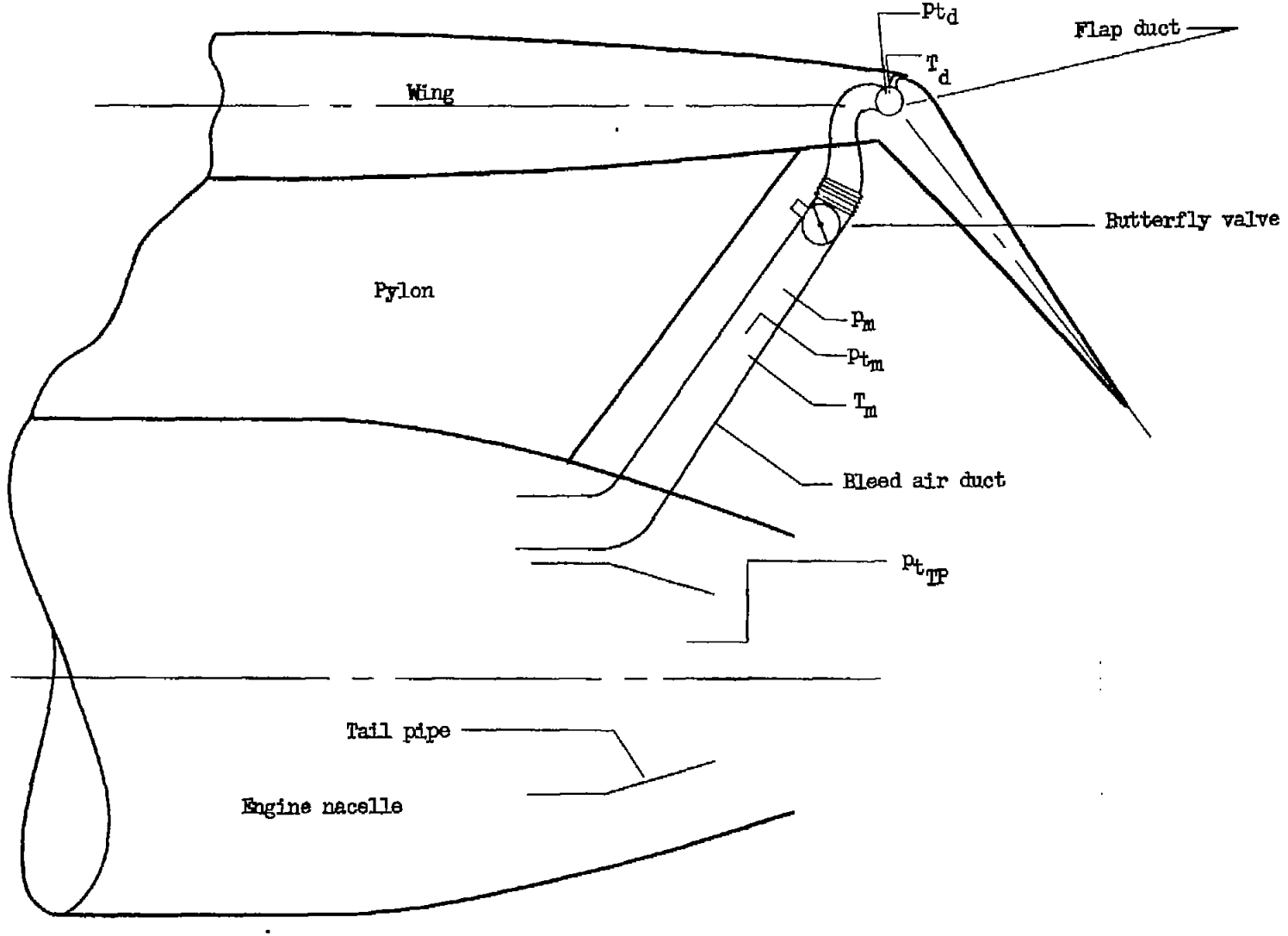

Figure 5.- Diagram of the engine bleed flow and thrust-measuring system.

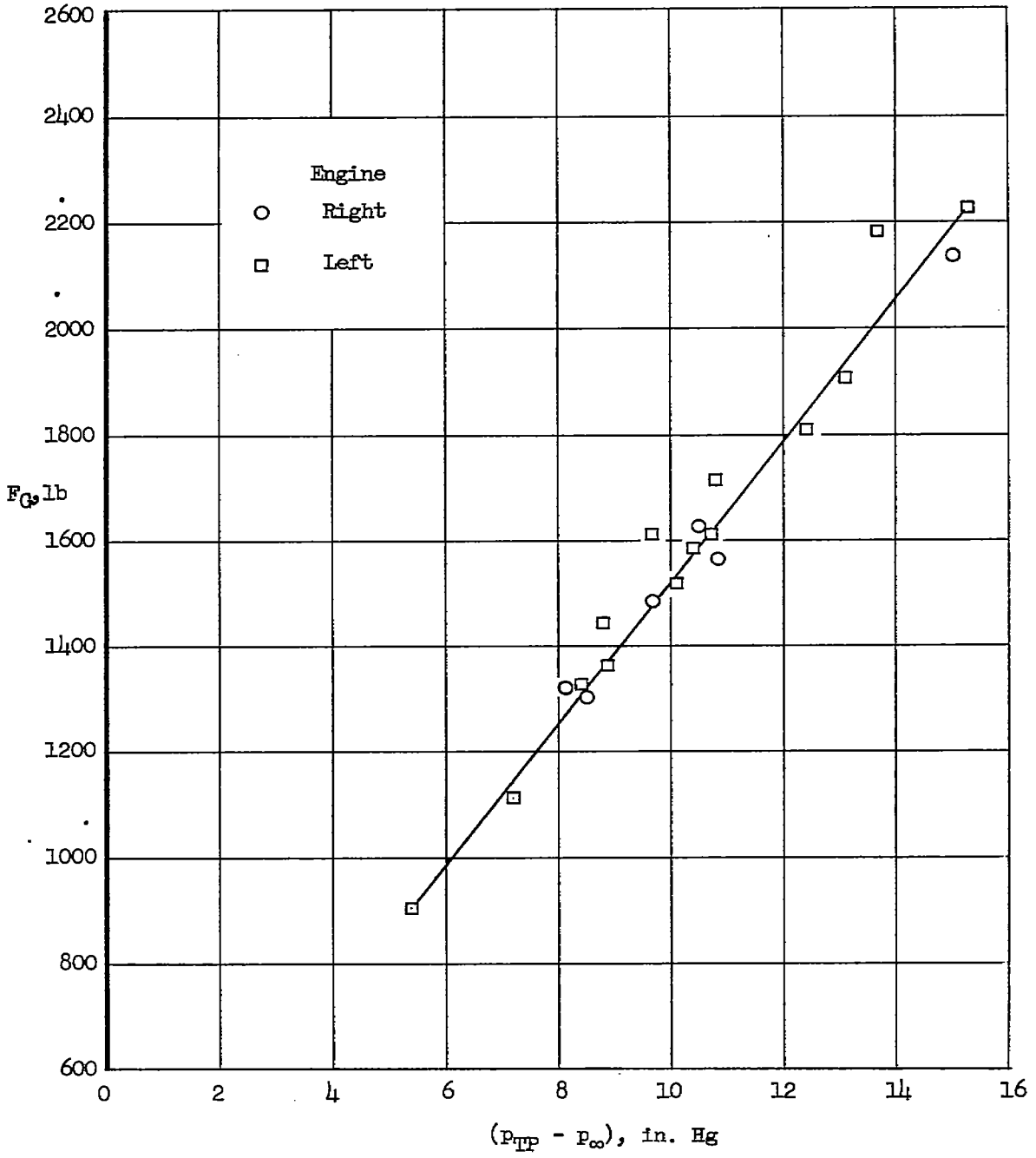

Figure 6.- Engine thrust calibration curve.

[redacted]

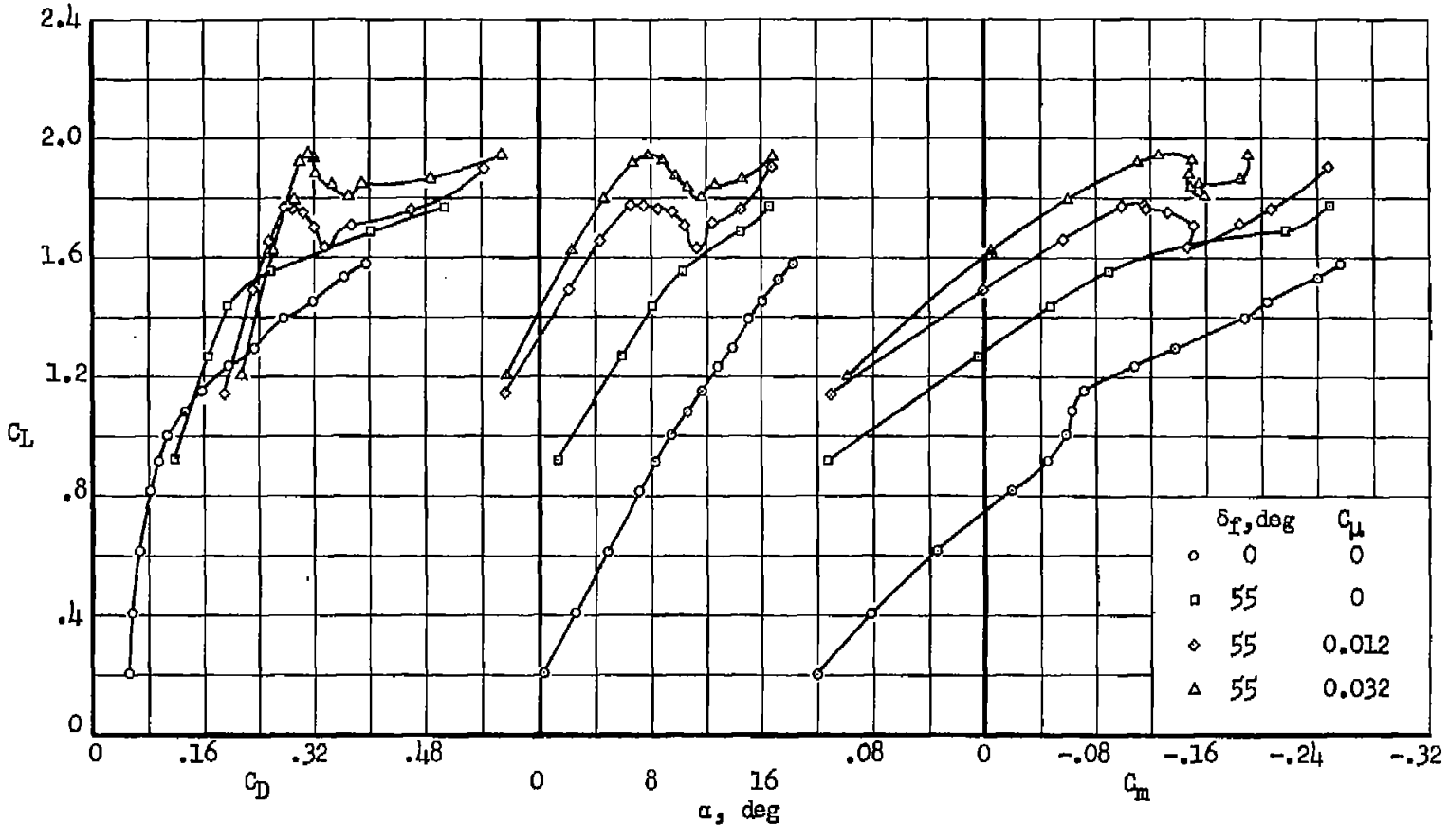

Figure 7.- Longitudinal characteristics of the basic configuration with and without blowing; normal airplane slat extended.

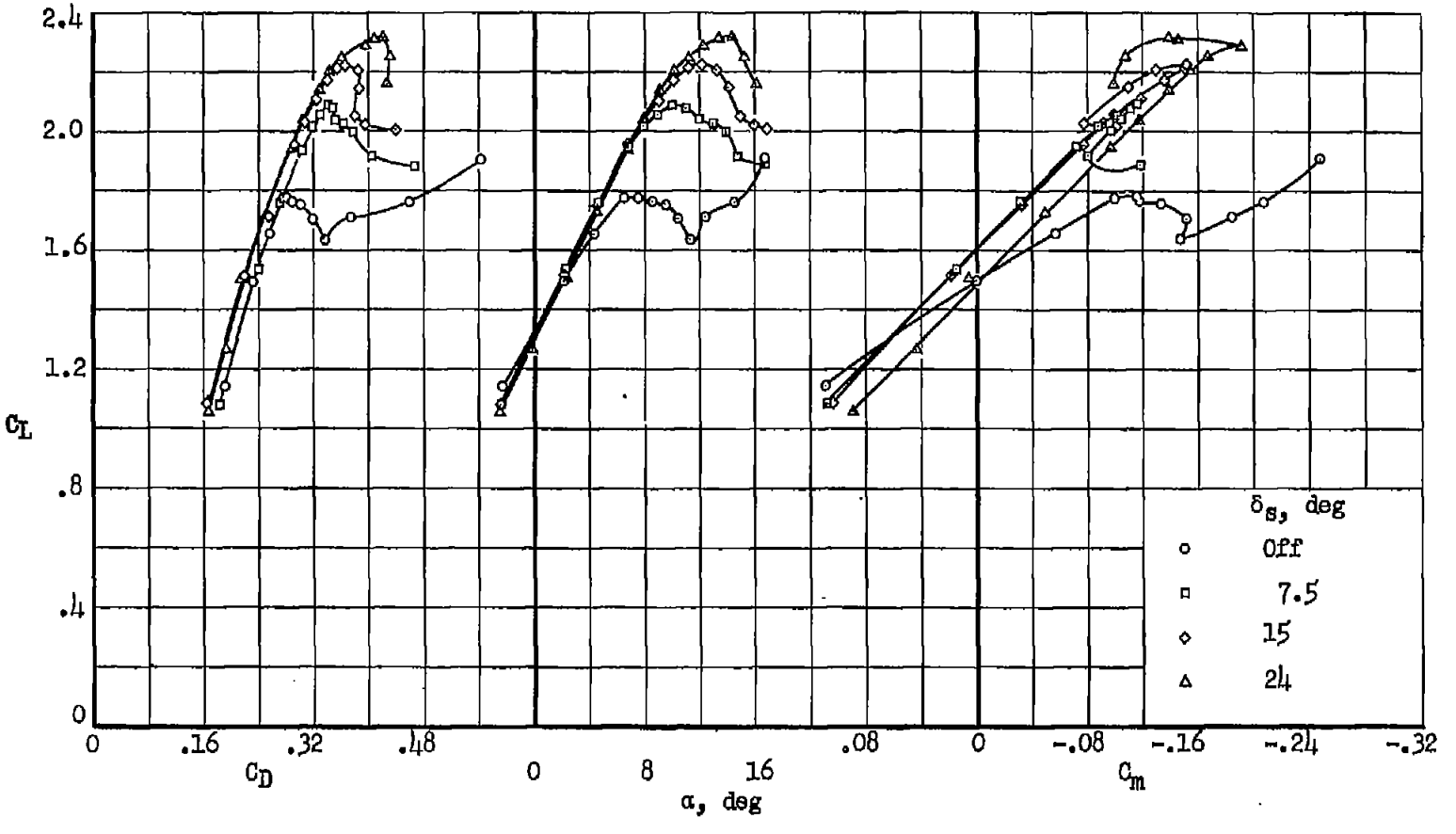

Figure 8.- Longitudinal characteristics of the airplane with an inboard slat, M_2, in combination with the normal airplane slat; $\delta_f = 55^\circ$, $C_\mu = 0.012$.

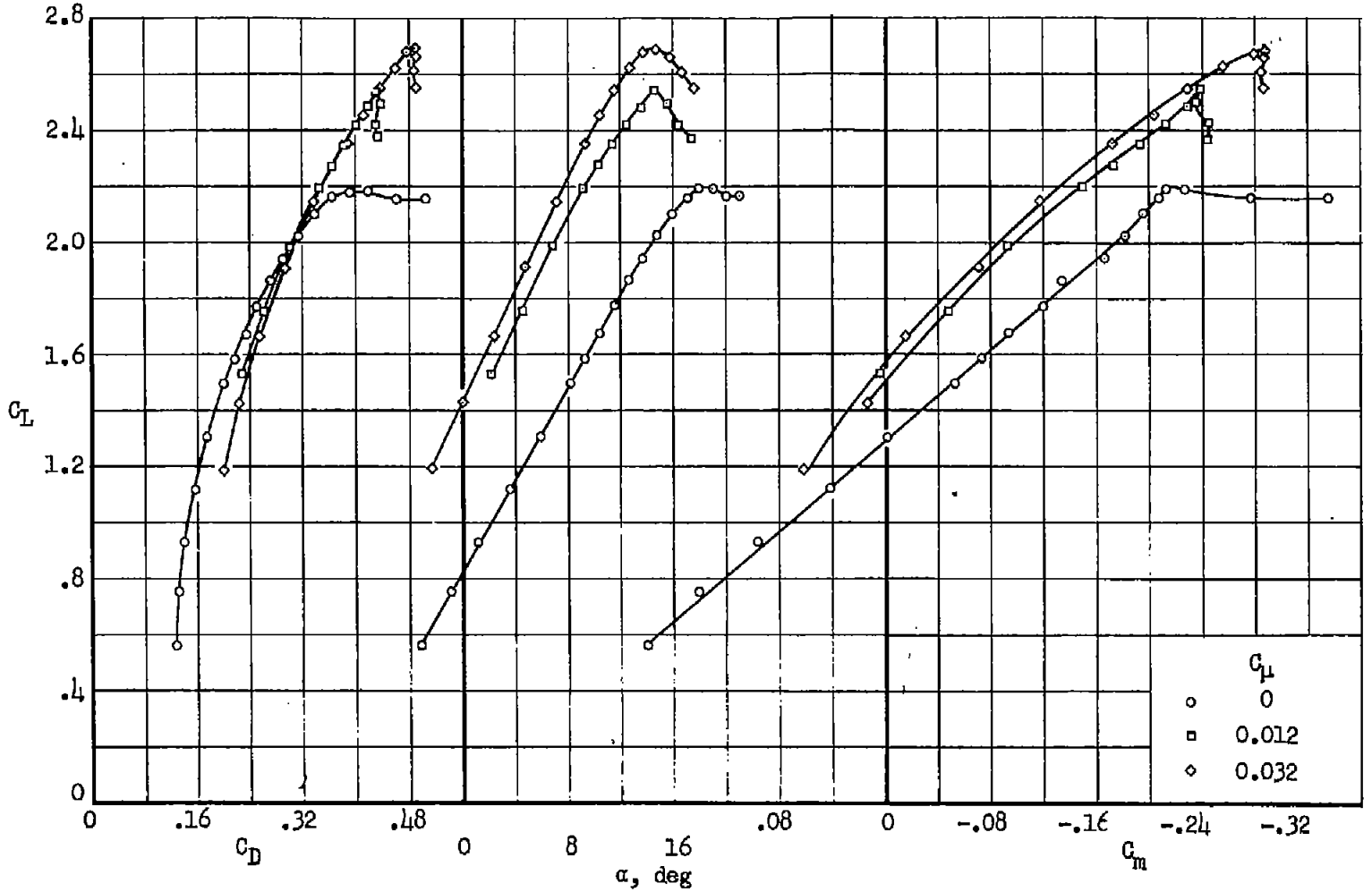

Figure 9.- Longitudinal characteristics of the airplane with full-span simulated 24° slat $M_2 + M_3$; $\delta_f = 55°$.

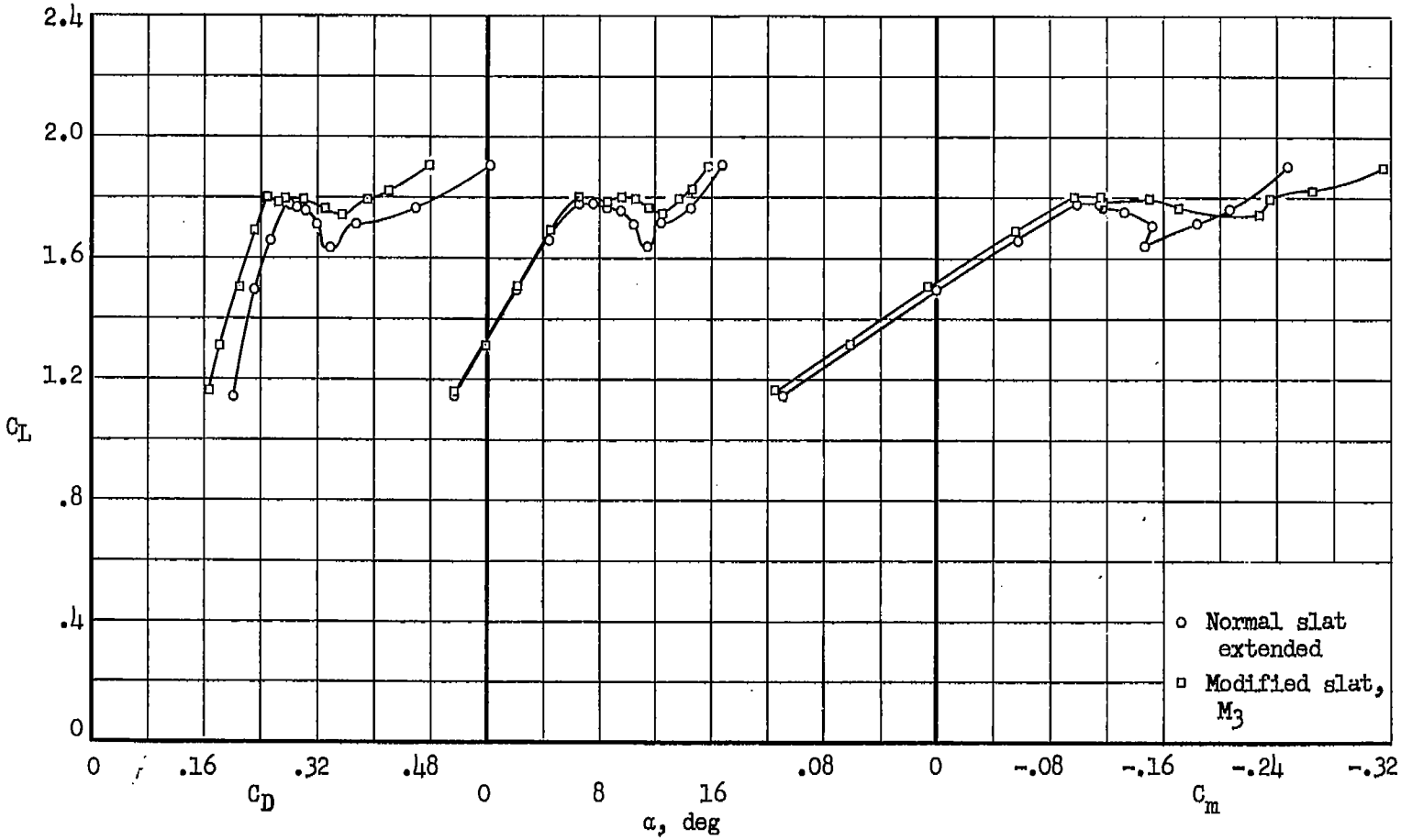

Figure 10.- Longitudinal characteristics of the airplane with and without a simulated 24° slat outboard of the nacelle pylons in combination with normal wing inboard; $\delta_f = 55°$, $C_\mu = 0.012$.

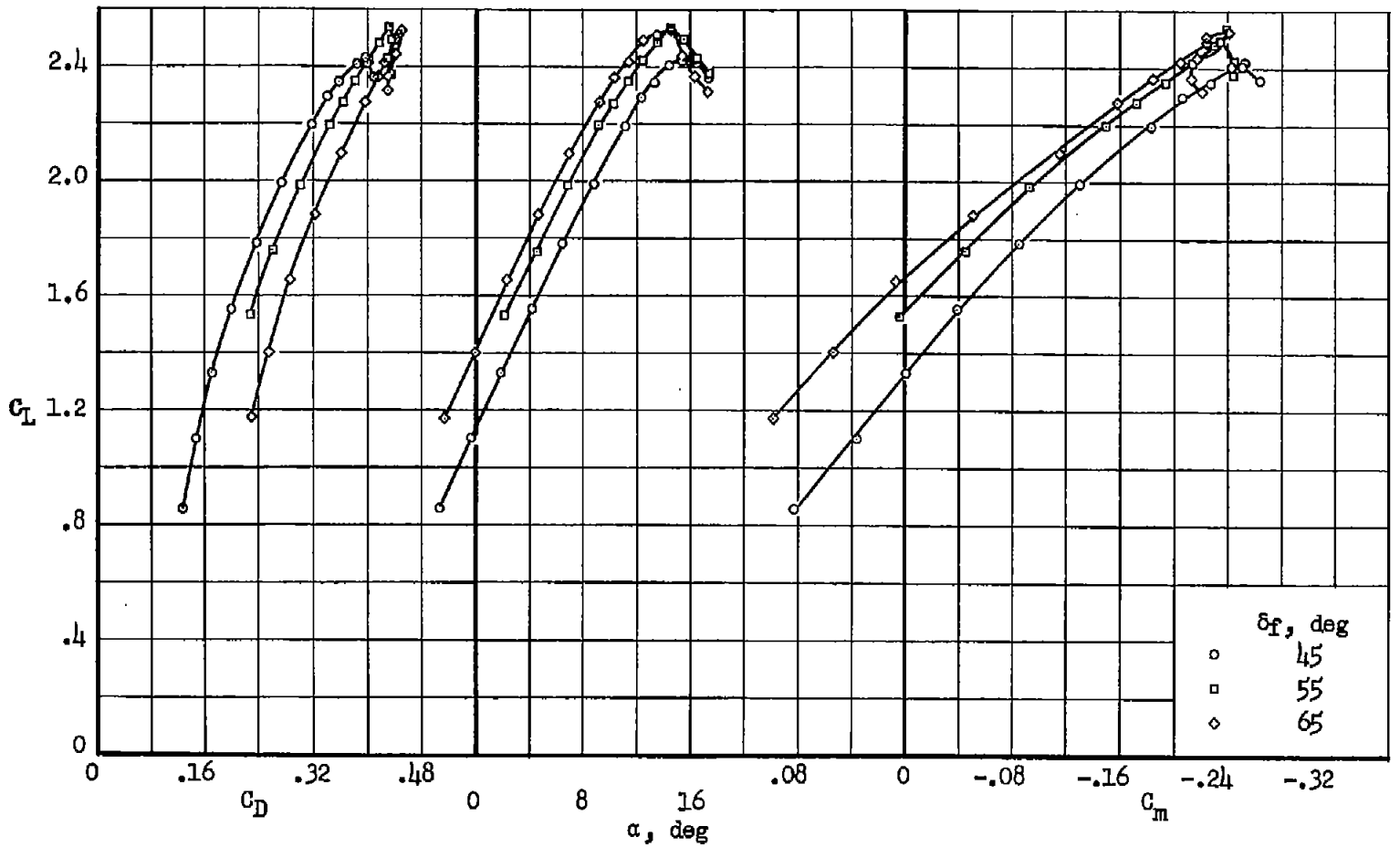

Figure 11.- Effects of flap deflection angle with full-span simulated 24° slat modifications, $M_2 + M_3$, on the longitudinal characteristics of the airplane; $C_\mu = 0.012$.

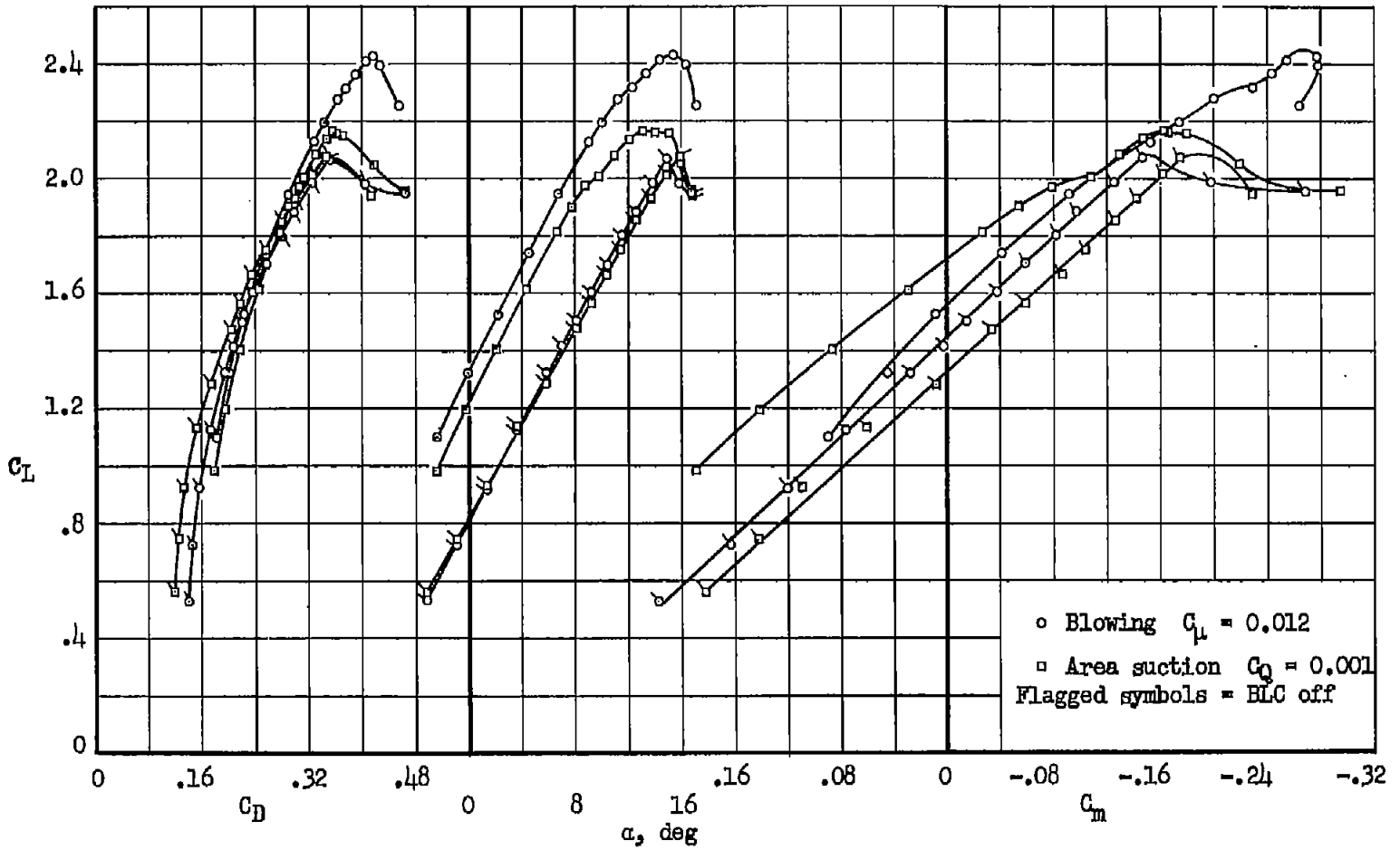

Figure 12.- A comparison of the characteristics of the airplane with area-suction and blowing flaps deflected 55°; inboard glove modification in combination with outboard simulated 24° slat, $M_1 + M_3$.

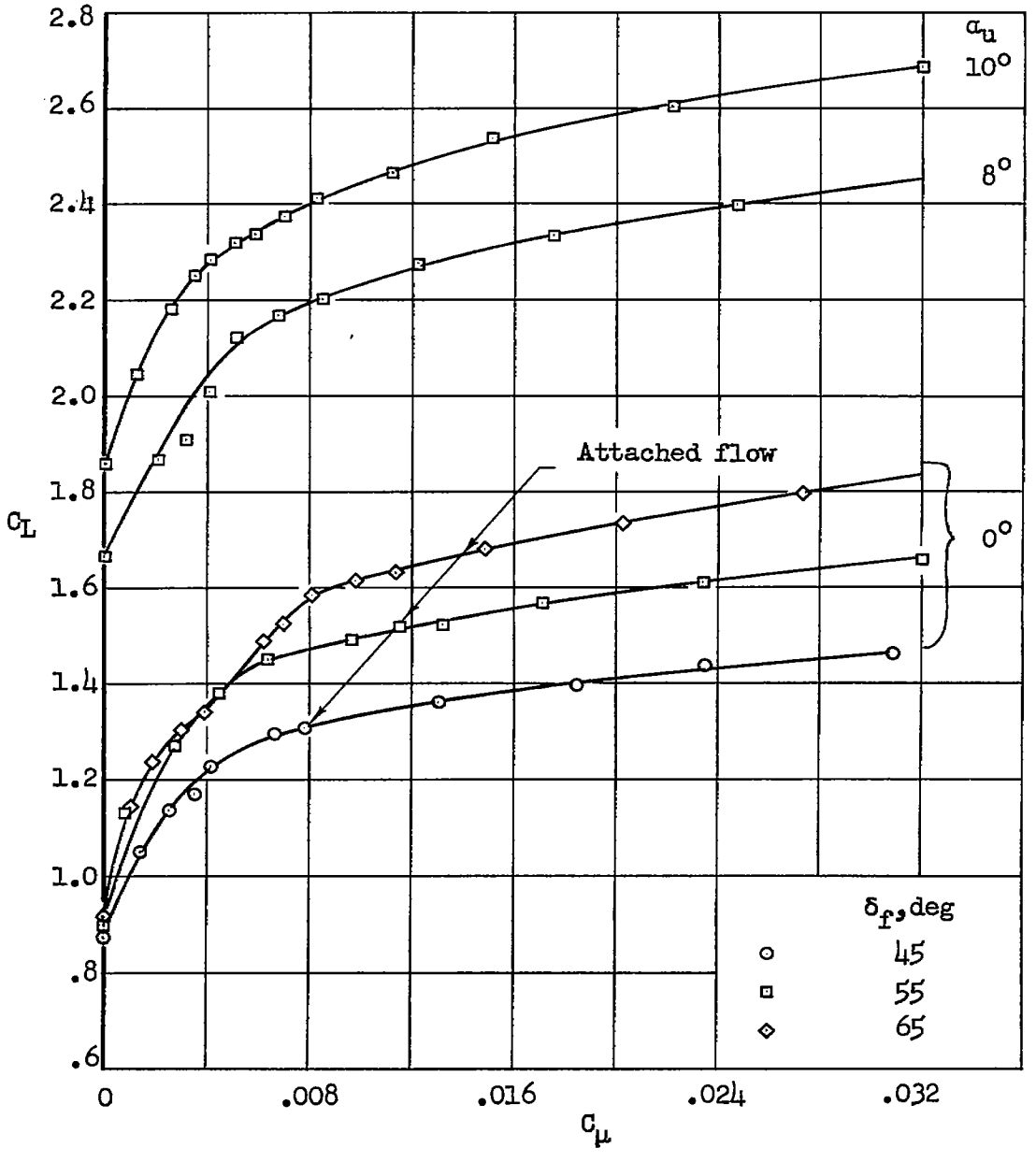

(a) C_L vs. C_μ

Figure 13.- Variation of lift coefficient with momentum, flow, and duct pressure coefficients at several flap deflections with full-span simulated 24° slat modifications $M_2 + M_3$.

[redacted]

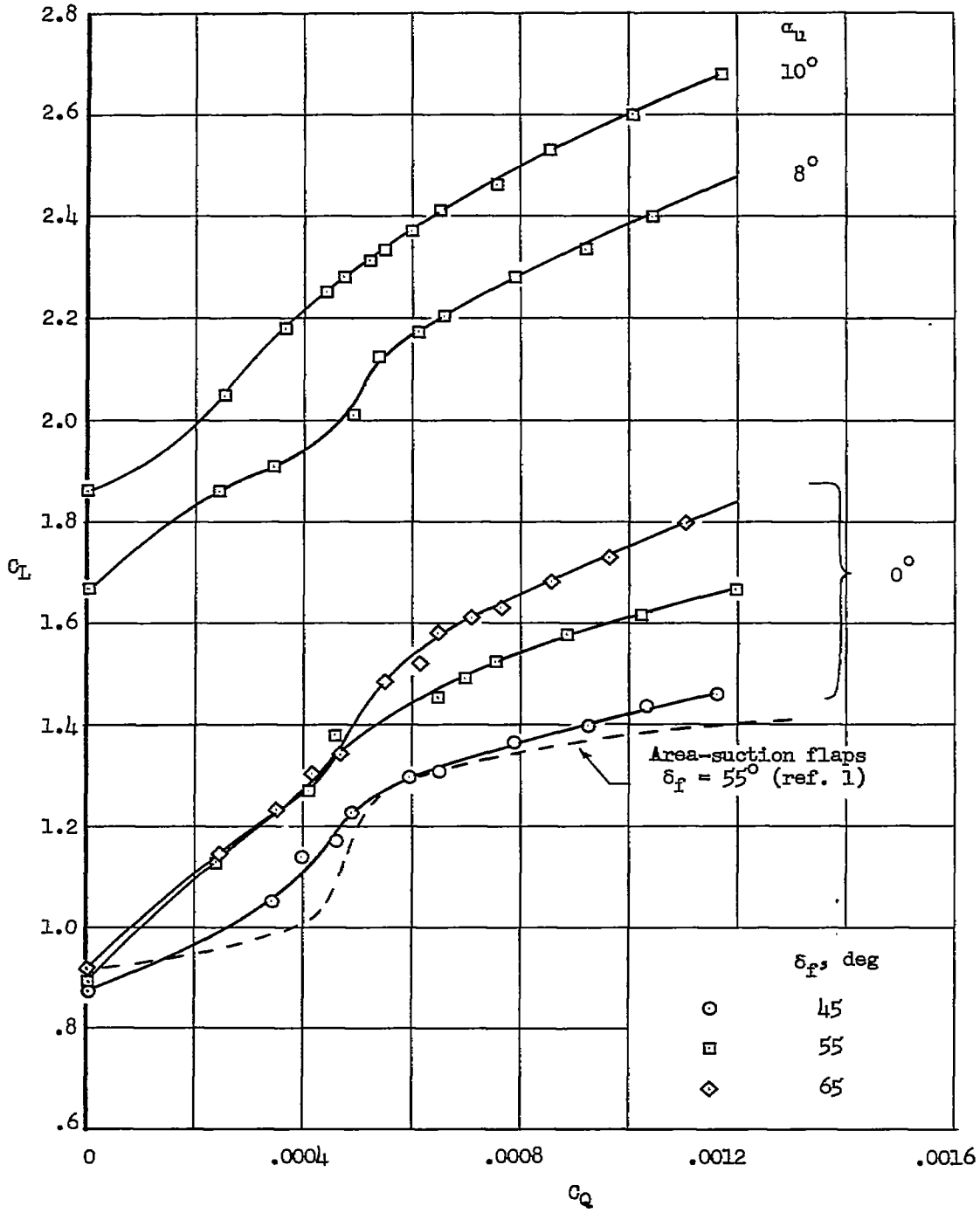

(b) C_L vs. C_Q

Figure 13.- Continued.

[redacted]

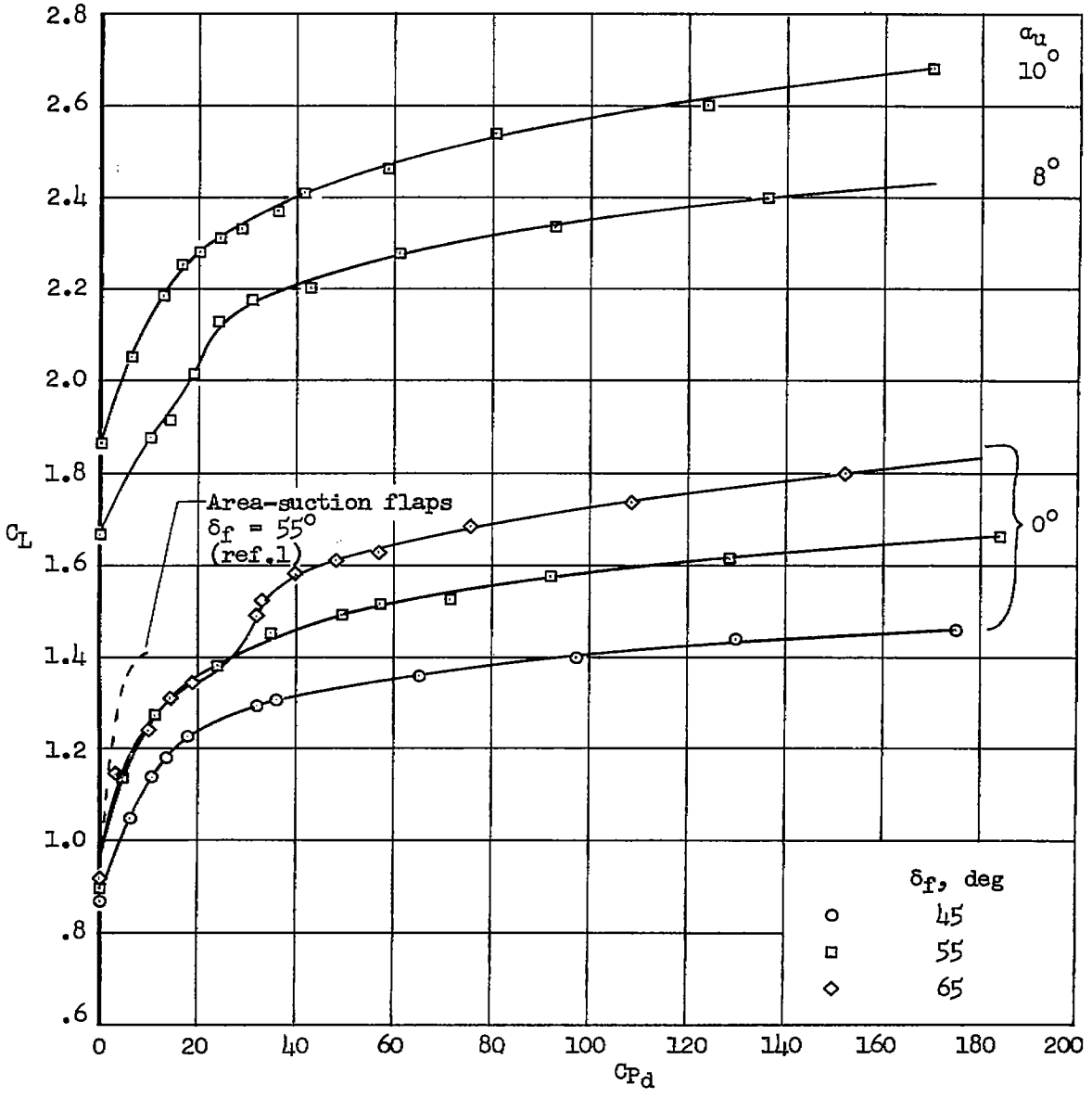

(c) C_L vs. C_{P_d}

Figure 13.- Concluded.

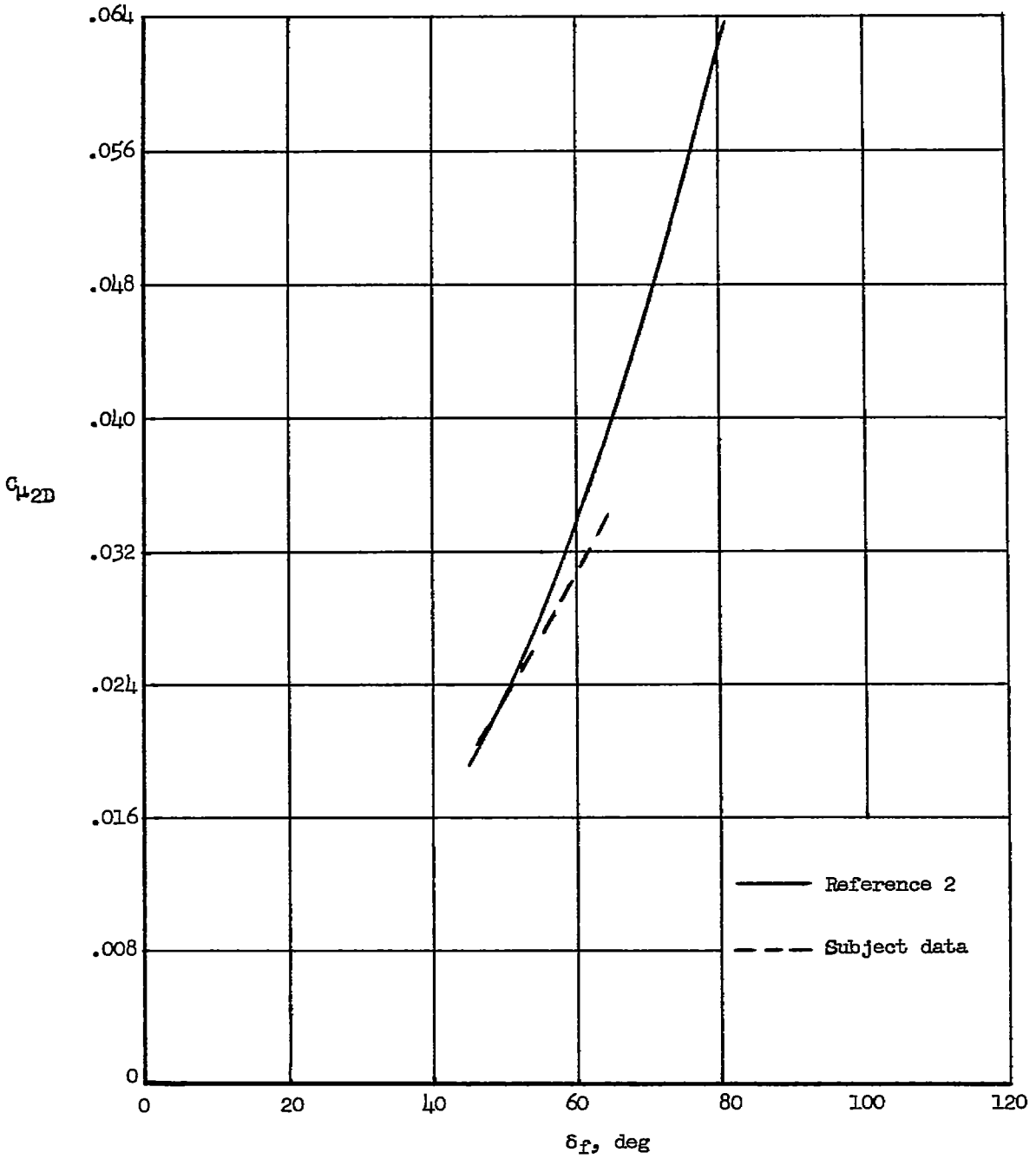

Figure 14.- Comparison of equivalent two-dimensional values of momentum coefficient for attached flow with values from reference 2.

[redacted]

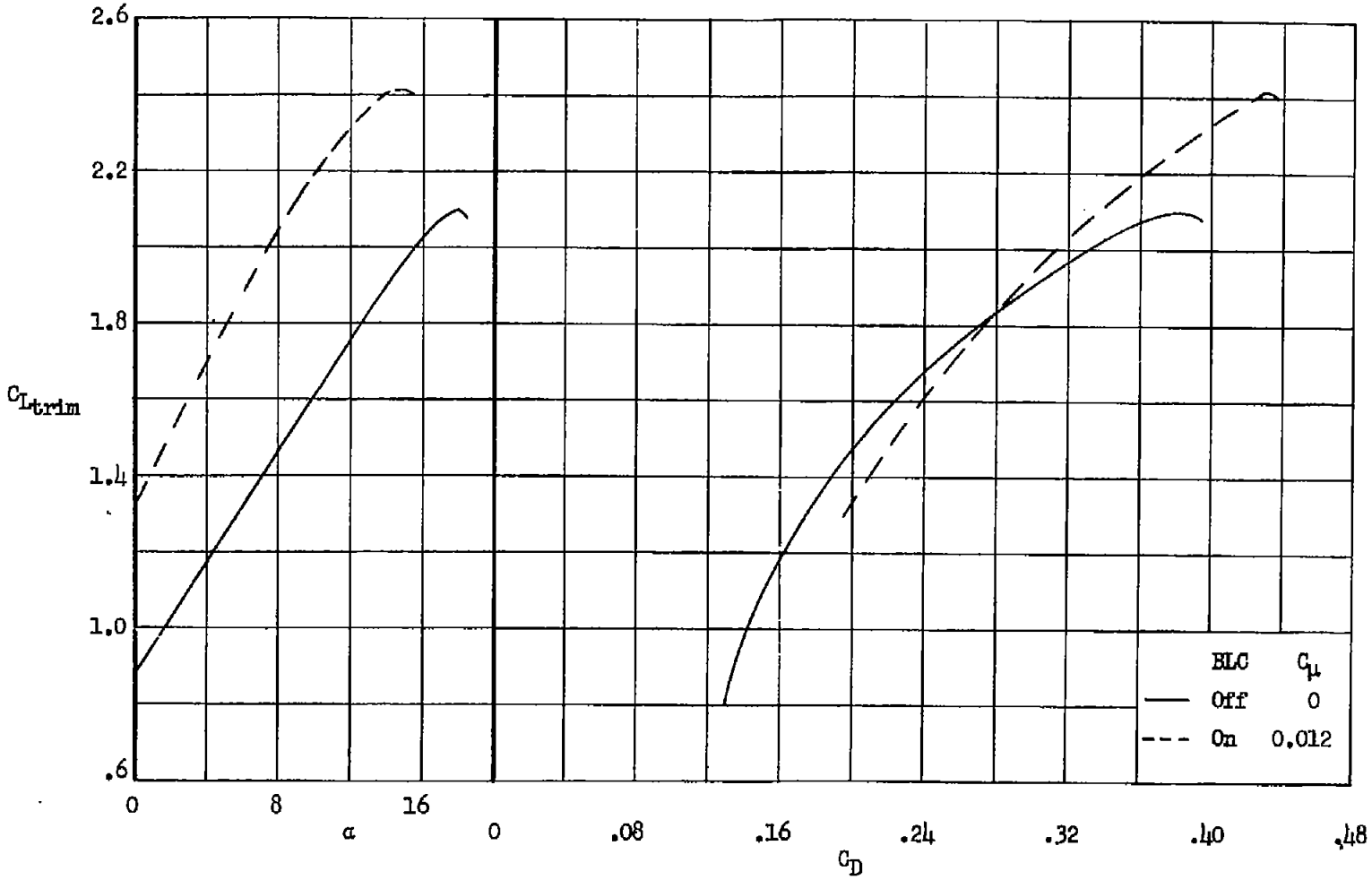

Figure 15.- Variation of trimmed lift coefficient with angle of attack and drag coefficient as used for performance calculations; full-span simulated 24° slat $M_2 + M_3$, $\delta_f = 55°$.

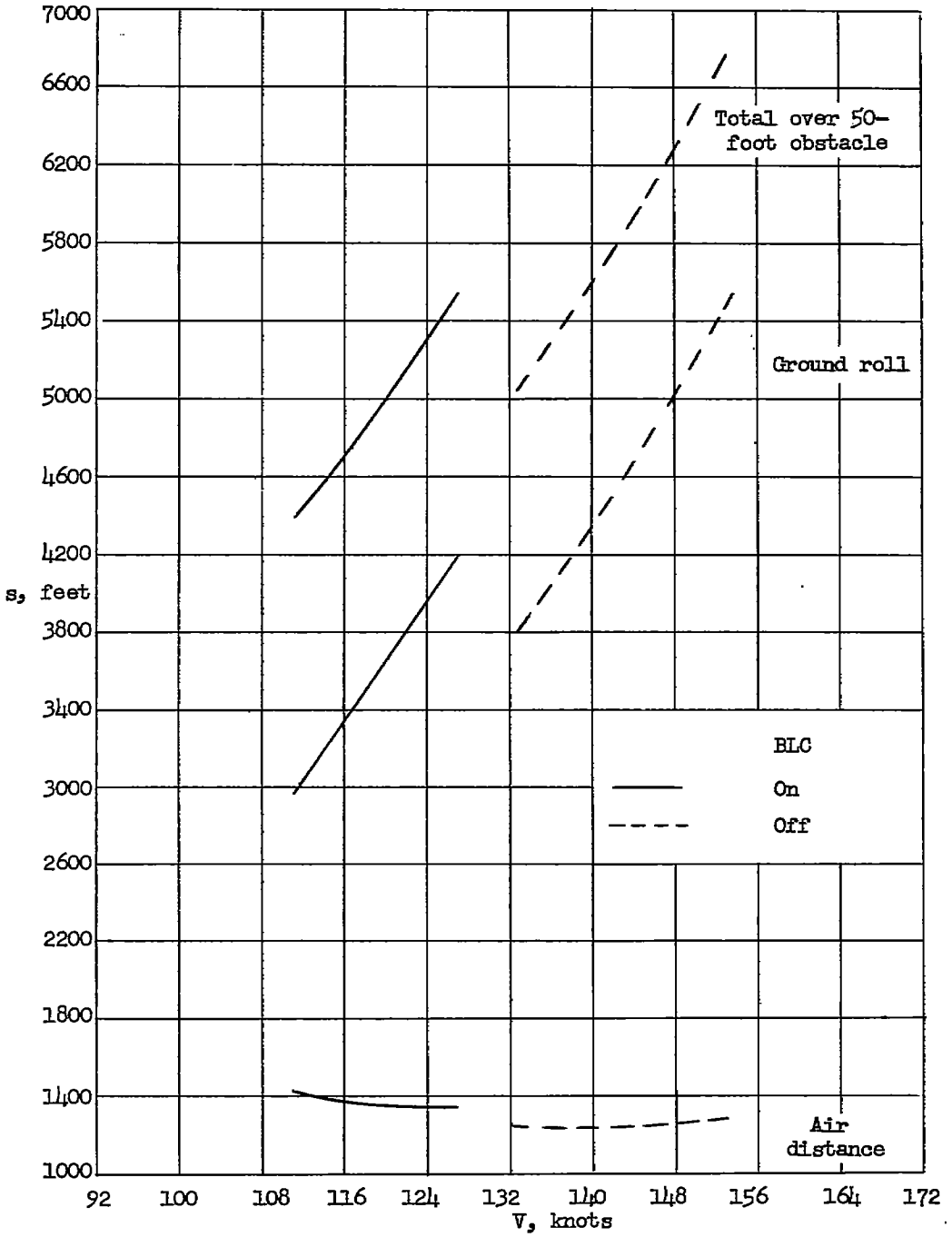

Figure 16.- Estimated take-off distances at various speeds with and without blowing; W/S = 90 lb/sq ft, full-span simulated 24° slat $M_2 + M_3$, $\delta_f = 55°$.

[redacted]

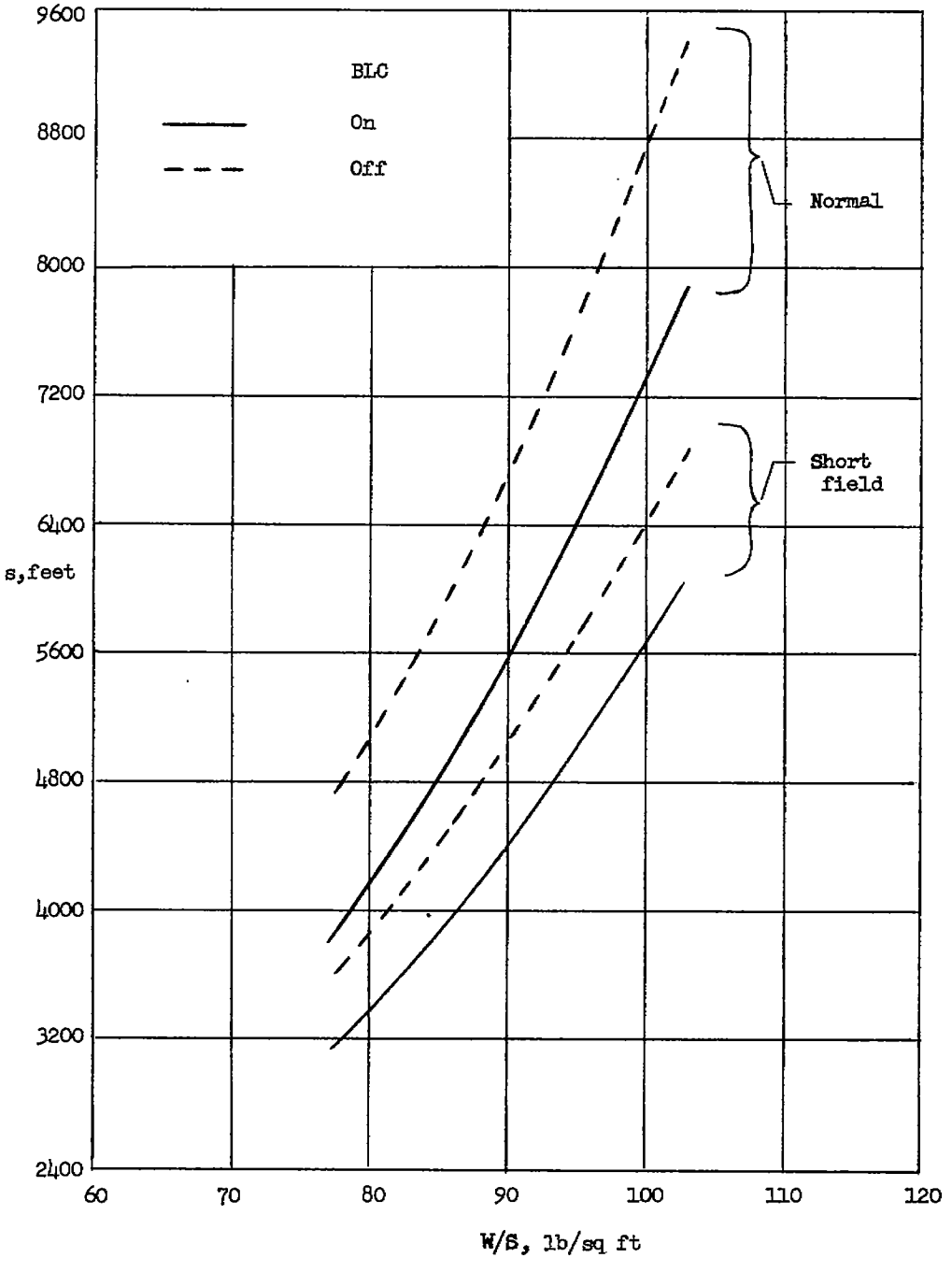

Figure 17.- Calculated total take-off distance over a 50-foot obstacle at various wing loadings; full-span simulated 24° slat $M_2 + M_3$, $\delta_f = 55°$.

[redacted]

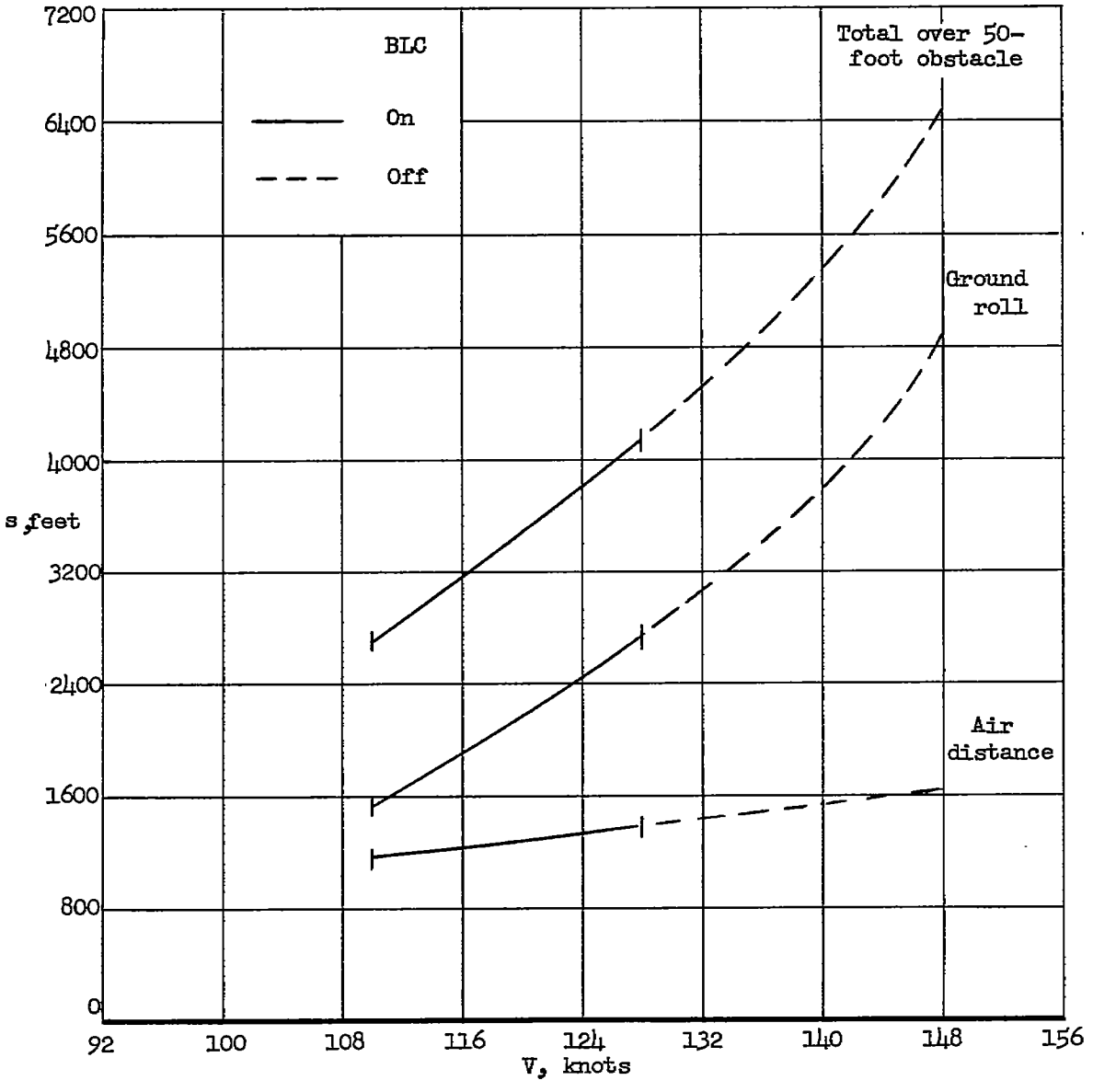

Figure 18.- Calculated landing distances at various approach speeds with and without blowing; W/S = 64.1 lb/sq ft, full-span simulated 24° slat $M_2 + M_3$, $\delta f = 55^\circ$, V_{v_1} = -15 ft/sec.

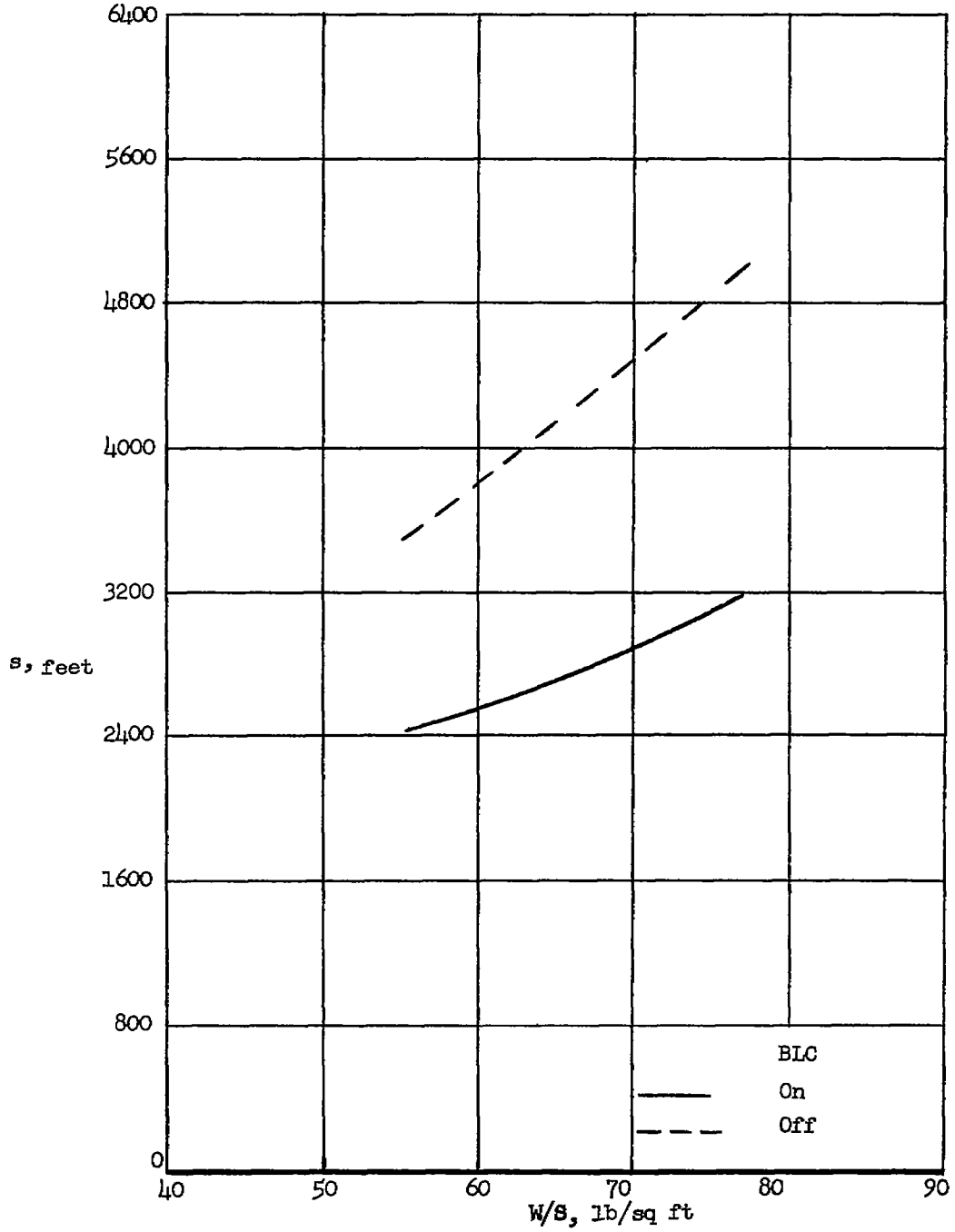

Figure 19.- Calculated minimum total landing distance over a 50-foot obstacle at various wing loadings; full-span simulated 24° slat $M_2 + M_3$, $\delta_f = 55°$, $V_{v_1} = -15$ ft/sec.

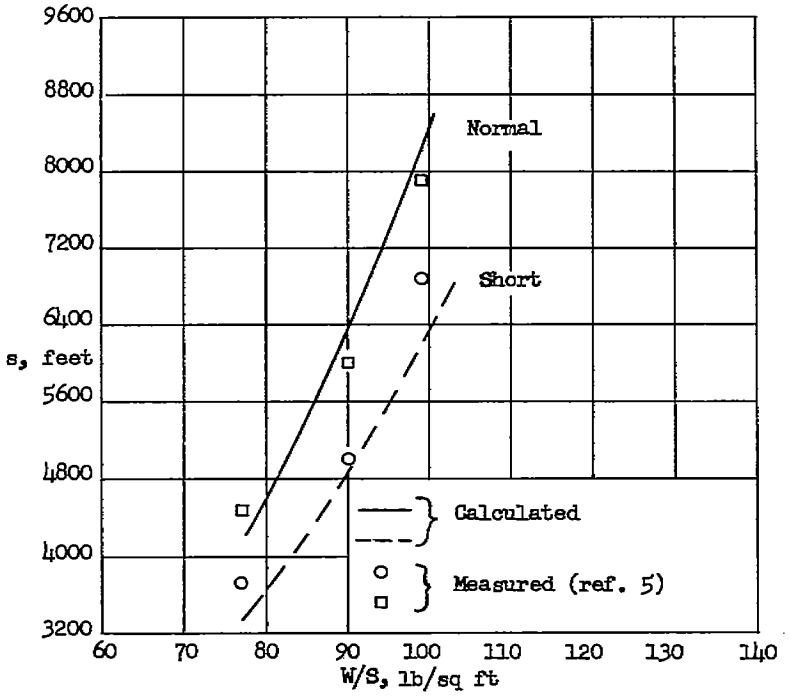

(a) Take-off.

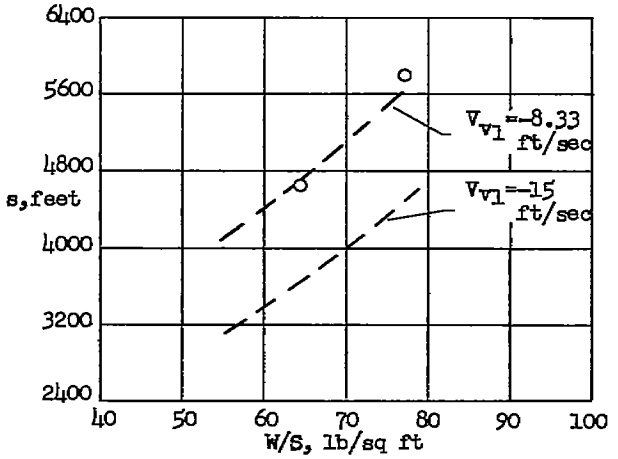

(b) Landing.

Figure 20.- Comparison of calculated landing and take-off distances at various wing loadings for the airplane equipped with 36° slotted flaps and partial-span slats with flight-test results (ref. 5) of a similar airplane.

[redacted]

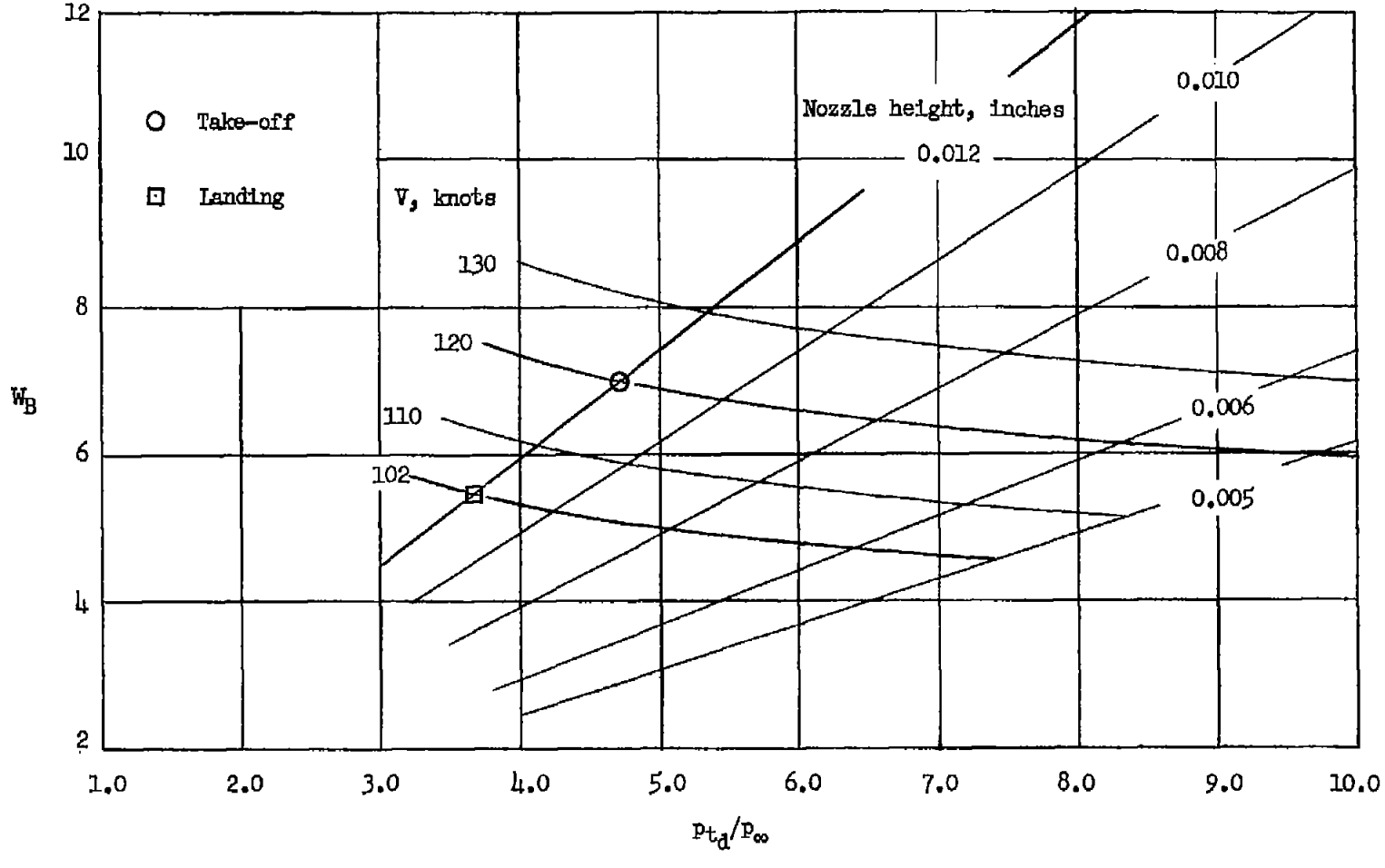

Figure 21.- Calculated bleed-air requirements for the subject airplane for various airspeeds and nozzle sizes to give $C_\mu = 0.011$; $T_d = 860^\circ$ R.

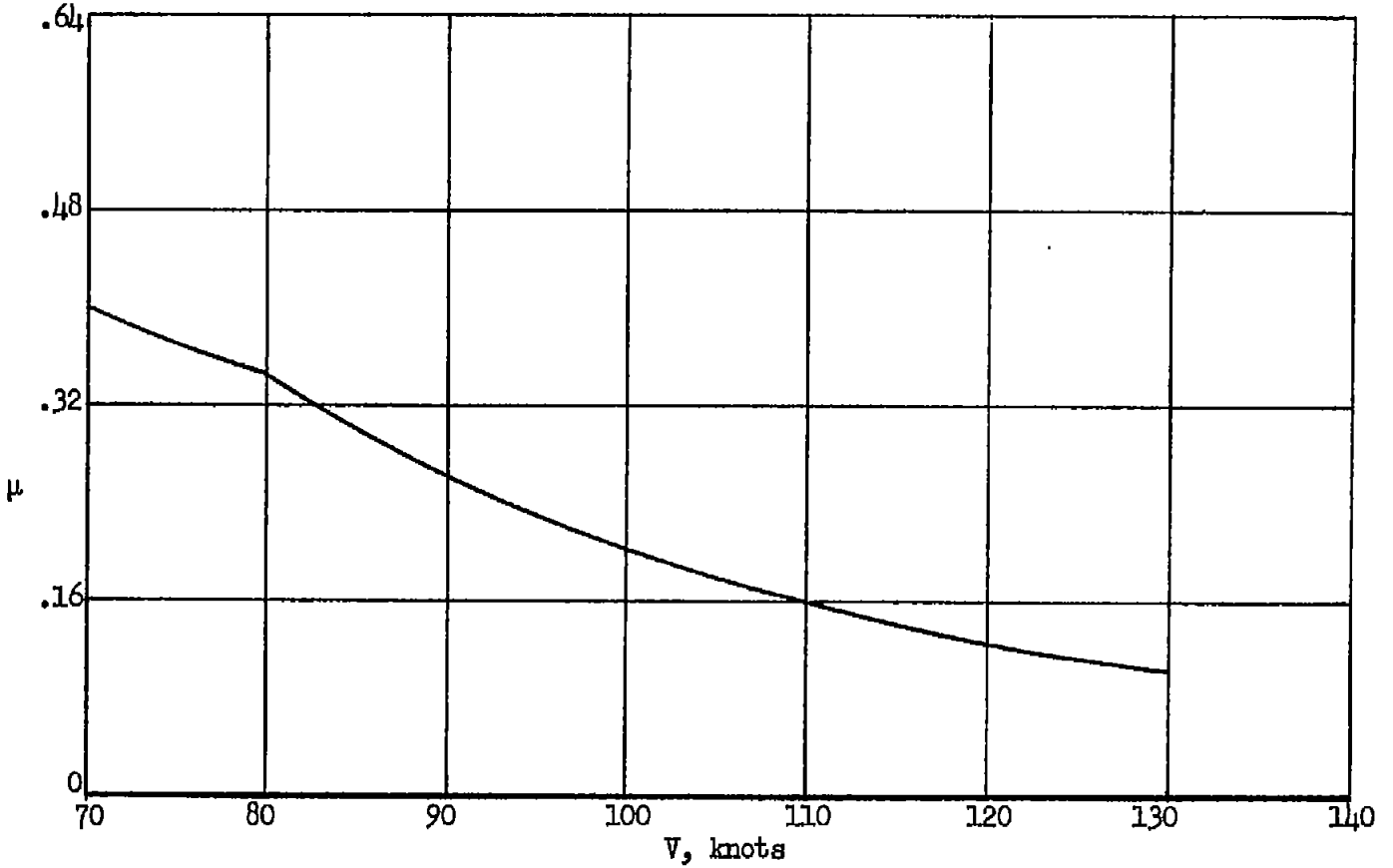

Figure 22.- Variation of braking coefficient with speed, reference 9.